Comparative Planetary Circulation Regimes with a Simplified GCM

DPhil 1st Year Report

Yixiong Wang

Atmospheric, Oceanic and Planetary Physics
Department of Physics

St Cross College

University of Oxford

Supervisor: Professor Peter Read

Word count: 10352

Abstract

This report presents the first year's work of my DPhil project. The overall objective of this project is to establish a parameter space in which the dependence of terrestrial planetary circulation regimes are mapped with respect to defining dimensionless parameters. In this report, an overview of the diversity of the Solar System terrestrial planetary circulation regimes is presented, with accompanying theories developed for general circulation dynamics. Previous laboratory and numerical studies on the parameter dependence of rotating flow regimes are reviewed, and the corresponding characteristic dimensionless parameters are introduced. The simplified GCM—PUMA (Portable University Model of Atmospheres) is used in this project to act as the prototype atmosphere to conduct generic controlled experiments. The influence of the planetary rotation rate on the global circulation regime is studied systematically with various diagnostic results analysed. Experiments over a wide range of rotation rate from $8\Omega_E$ to $1/16\Omega_E$ are performed (Ω_E is the Earth's rotation rate). Results of this simplified GCM show very similar trends to those found in the GCM's laboratory counterpart as well as to the observational features of Solar System planets. Future work will further explore the parameter space, by studying the influence of radiative properties of the atmosphere, obliquity of the planet's spin-axis, as well as some extreme conditions such as a tidally-locked orbit.

Contents

1 Introduction **4**
- 1.1 The Problem . . . 4
- 1.2 General Approach . . . 6
- 1.3 Chapter Introductions . . . 7

2 Diversity of Planetary Atmospheric Circulation **8**
- 2.1 Overview of the Terrestrial Circulation Theories . . . 8
  - 2.1.1 Hadley Cell Dynamics . . . 9
  - 2.1.2 Baroclinic Waves and Eddies . . . 12
- 2.2 Earth and Mars . . . 15
- 2.3 Venus and Titan . . . 17

3 Parameter Dependence Study **19**
- 3.1 Laboratory Experiments . . . 19
  - 3.1.1 Apparatus and Configuration . . . 19
  - 3.1.2 Non-dimensional Parameters and Flow Regimes . . . 20
- 3.2 Numerical Experiments . . . 22
  - 3.2.1 Non-dimensional Parameters . . . 22
  - 3.2.2 Circulation Regimes in Model Simulation . . . 25

4 PUMA **30**
- 4.1 Model description and dynamics . . . 30
  - 4.1.1 Dynamical core . . . 30
  - 4.1.2 Parameterisation of physical processes . . . 34
- 4.2 Experiment design and configuration . . . 36

5 Diagnostic Results **38**
- 5.1 Spin-up . . . 38
- 5.2 Zonal mean field diagnostics . . . 39
- 5.3 Non-axisymmetric features—eddies and waves . . . 43

5.4 Runs with a smaller planetary radius 56
5.5 Discussion on dimensionless numbers 58

6 Conclusions and Future Work **60**
6.1 Conclusions 60
6.2 Future Work 61
6.3 Preliminary Timetable 63

Chapter 1

Introduction

I think the Causes of the General Trade–Winds have not been fully explained by any of those who have wrote on that Subject...
— George Hadley (1735)

1.1 The Problem

The study of atmospheric general circulation, which dates back to the 18th century with the pathbreaking work by *Hadley* [1735], has been greatly enriched by explorations (both observational and theoretical) of other planets since the last century. Within our solar system, substantial atmospheres were discovered on a series of planetary bodies: Venus, Mars, the gas/ice giants (Jupiter, Saturn, Uranus and Neptune), and Titan—the largest moon of Saturn (see Table 1.1). Our knowledge of the dynamics, radiative properties, and chemical compositions of these planets as well as the atmospheres wrapping them have grown to a reasonably satisfactory extent, by means of ground-based, orbital and in-situ observations. Beyond the kingdom of the Sun, more than 400 extrasolar planets (more popularly known as Exoplanets) have been detected using various astronomical observation techniques, and many of them are believed to hold atmospheres around (see http://exoplanet.eu/). The differences of climate and circulation amongst these planetary atmospheres are strikingly significant. Even our two nearest neighbours pose an impressive contrast: a hot (read: melting) and high pressure (100 times of the Earth!) inferno on Venus versus a cold (read: frozen) and extremely low pressure (1% of the Earth!) desert–world on Mars.

From a physicist's viewpoint, all of these planetary atmospheres can be abstracted as rotating, stratified fluids moving under mechanical, radiative

Planet	g ($\times g_E$)	Albedo (%)	Surface temperature (K)	Surface pressure (bar)	Atmospheric composition
Venus	0.905	75	737	92	$96.5\%CO_2, 3.5\%N_2$ $0.015\%SO_2, 0.002\%H_2O$
Earth	1.000	30.6	288	1	$78\%N_2, 21\%O_2,$ $0.038\%CO_2, < 1\%H_2O$
Mars	0.379	25.0	184 night,242 day	0.004-0.009	$95.3\%CO_2, 2.7\%N_2,$ $0.021\%H_2O$
Jupiter	2.530	34.3	165	$\gg 1000$	$89.8\%H_2, 10.2\%He,$ $0.3\%CH_4, 0.026\%NH_3$
Saturn	1.065	34.2	134	$\gg 1000$	$96.3\%H_2, 3.25\%He,$ $0.45\%CH_4, 0.0125\%NH_3$
Uranus	0.905	30.0	76	$\gg 1000$	$82.5\%H_2, 19.0\%He,$ $1.5\%CH_4$
Neptune	1.14	29.0	72	$\gg 1000$	$80.0\%H_2, 19.0\%He,$ $1.5\%CH_4$
Titan	0.14	22.0	93.7	1.47	$98.4\%N_2, 1.4\%CH_4,$ $0.1\%H_2$

Table 1.1: Basic properties of the planetary atmospheres within Solar System (Note: Surface temperature of gas giants refers to the temperature at 1bar level)

and electromagnetic forcings from the host star and the underlying planet. It is thus natural to ask the question that what characteristic factors most fundamentally determine the various circulation patterns that we observe in those exotic worlds, and whether it is possible for us to predict the climate conditions there based on limited observational information and our knowledge of the general circulation.

The meaning of giving a complete answer to this question is not just to satisfy our sheer intellectual curiosity. The understanding of the dominating factors and mechanisms of the general circulation is a prerequisite to our understanding of the climate variability of the Earth both in the past and in the future. Besides, light could be shed on the potential habitability questions of exoplanets by studying the parameter dependence of the general circulation regime. Given the launch of the NASA Kepler mission

(see http://www.kepler.arc.nasa.gov/) in 2009 as well as rapidly growing ground-based observations, more and more Earth-like terrestrial exoplanets (although most of them are Super Earths perhaps, see *Irwin et al.* [2009]) are expected to be discovered(see *Selsis et al.* [2007]), thus lending great relevance to the study of such fundamental issues.

1.2 General Approach

The general methodology employed by most theoreticians for this sort of problem is to establish a model atmosphere which is usually built upon various reasonable idealisations, and then gain insights by studying the behaviours of this model atmosphere. In most cases, simple models incorporating dynamic constraints and key physical processes are used rather than the highly complex and 'realistic' models with great details (full GCMs). This is of course partly for the convenience of handling, but more importantly, because it tells us more about physics and causal relationships, which are usually not explicitly expressed in the results of complex models. By conducting sequences of controlled experiments and sensitivity tests on these simple models (either numerical or laboratory), dominating factors for the formation and maintenance of circulation regimes can be highlighted.

Laboratory analogues of planetary atmospheres usually take the form of viscous stratified fluids confined within a rotating annulus(or tank) heated or cooled from the boundaries. This configuration, although devoid of spherical geometry and radiative processes, captures the essential physics of the atmospheric circulation, that is, rotating fluids under the forcing of differential stellar heating. Since the pioneering work of *Hide* [1953] and *Fultz et al.* [1959], much knowledge of the general circulation as well as other aspects of atmospheric dynamics has been gained by studying these flow patterns (see *Hide and Mason* [1975], *Lorenz* [1969]). Flow behaviours under various conditions have been thoroughly measured and classified, and their dependence on non-dimensional parameters can be shown by mapping the flow patterns within a parameter space (the map you get is known as a regime diagram). Nowadays this method is still continuously providing considerable enlightenment (both for scientific research and for education) in the study of geophysical fluid dynamical systems (see *Read et al.* [1998], *Read* [2001], *Wordsworth et al.* [2008], *Illari et al.* [2009]).

Another approach is to make use of simplified numerical models of planetary atmospheres to investigate the behaviour of the circulation. There have been a series of studies taking the parameter approach to study model

circulations since the 1970s (see *Hunt* [1979], *Williams and Holloway* [1982], *Geisler et al.* [1983], *Del Genio and Suozzo* [1987], *Williams* [1988a], *Williams* [1988b], and *Jenkins* [1996]), with motivations ranging from paleoclimate simulation to GCM parameter tests. Usually the parameters available to be tuned within a simple GCM include planetary rotation rate, planetary radius, obliquity, etc. Thus similar (although perhaps more complicated) regime diagrams are expected to be produced by such numerical experiments. And some of the previous work does yield preliminary regime diagrams(*Geisler et al.* [1983]). However, a systematic investigation and exploration of the parameter space has not yet been made. And this is one of the major motivations of the present project.

In this project, we will use the simplified GCM—PUMA (Portable University Model of Atmospheres) developed by the Meteorological Institute, University of Hamburg to conduct controlled experiments and sensitivity tests on factors like planetary rotation rate, radiative relaxation timescales, Rayleigh frictional timescales and so on. Corresponding non–dimensional parameters are suitably defined to construct a multi–dimensional parameter space in which circulation regimes are mapped.

1.3 Chapter Introductions

In this report, we first present an overview of the classical theories developed for the terrestrial atmospheric circulation, with a brief summary of the observed circulation features on rocky planets within our Solar System in Chapter 2. Chapter 3 then reviews the previous efforts (both laboratory and numerical method) taking parametric approach in the field of geophysical fluid dynamics. Chapter 4 describes the model dynamics and physics of PUMA, as well as the experiment setup and configuration. Chapter 5 presents the diagnostic results obtained during my first year. A summary of the conclusions and plans for the future work are discussed in Chapter 6.

Chapter 2

Diversity of Planetary Atmospheric Circulation

It is conventional to divide the planetary circulation regimes into two basic categories when we consider the global scale atmospheric dynamics: regimes of terrestrial planets, and regimes of gas/ice giants. The latter ones differ significantly from the former ones mostly because of their lack of a well-defined solid planetary surface. Besides, most of these giants (with Uranus as an exception for example) are still emanating considerable radiation from their deep interior (this radiation comes from the heat released by the gravitational accretion during the planetary formation, see *Dowling* [1995]), making the giant planets' circulations at least partly driven by internal heat sources. Given such fundamental differences, we will mainly focus on the circulation regimes of terrestrial planets in this project.

2.1 Overview of the Terrestrial Circulation Theories

The dynamical explanations for the mechanisms concerning terrestrial planetary circulations have grown to a somewhat well-established extent, through constant efforts of studying Earth's meteorology as well as explorations of other rocky planets (Mars, Venus...) within our solar system. In principle, the nature of general circulation is a coupled dynamics-radiation problem (see Figure 2.1). The concept of a so-called 'atmospheric heat engine' is frequently used to illustrate this idea (*Barry et al.* [2002],*Peixoto and Oort* [1992]). Differential heating drives the meridional motion of the atmosphere, and this horizontal advection prevents the atmosphere from reaching a state

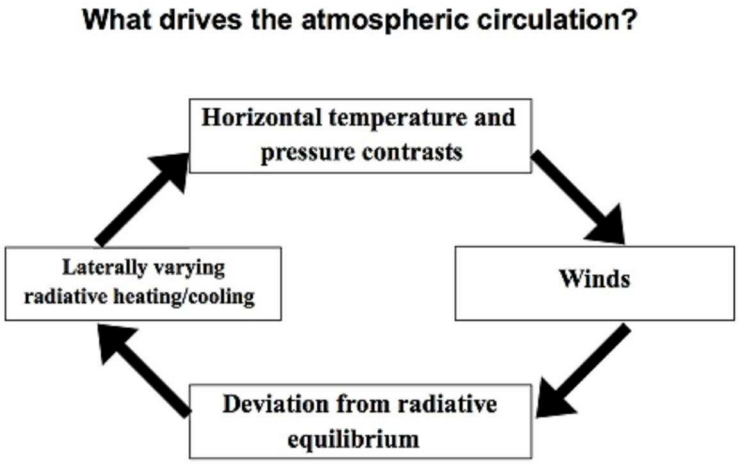

Figure 2.1: The nature of the general circulation, after *Showman et al.* [2010].

of local radiative equilibrium, thus leading to heating (cooling) at the equator (the poles), completing the energy cycle. Hadley (1735) first realised this point (that the circulation is driven by differential heating) and proposed an axisymmetric, meridionally circulating atmosphere to account for the prevailing trade winds over tropical regions. Subsequent observations then revealed that this overturning circulation (known as the 'Hadley Cell') is not dominating the whole hemisphere of the Earth. Instead, baroclinic waves and eddies are confirmed to be the major features of the extra-tropics. In the following, we will discuss tropical Hadley circulations and extratropical eddies separately, with a special focus on idealised analytical models devised to explain the corresponding mechanisms.

2.1.1 Hadley Cell Dynamics

The Hadley cell is axisymmetric (i.e. no longitudinal variation) without considering the longitudinal inhomogeneity of boundary terrain conditions. It serves as a reasonable approximation to the real circulation over tropics. This is different from the mid-latitude circulation where the inherent lon-

gitudinal variation brought by meandering waves and transient baroclinic eddies can not be neglected. As the most efficient way of transporting heat from hot tropics to cold poles, the Hadley cell commonly exists on nearly all terrestrial planets with substantial atmospheres that we have discovered.

Planetary rotation plays a crucial role in shaping the structure of Hadley circulation. It generally confines the Hadley cell within a limited range around the equator by exerting the constraint of angular momentum conservation (*Frierson et al.* [2007]). Taking Earth's atmosphere as an example, an air parcel free from longitudinal torques moving poleward will accquire a much greater velocity than we've observed before it reaches the mid-latidudes, leading to dynamical instability with meandering jets and waves. As we shall discuss in the following sections, on slowly rotating planets like Venus and Titan, Hadley cell occupies a far larger domain due to weak rotational effect.

In theoretical studies, simplified conceptual models are usually more enlightening than complex realistic ones. One of the most successful and illuminating models of the Hadley cell is that proposed by *Held and Hou* [1980]. Built upon a series of assumptions, like the small angle approximation, angular momentum conservation, geostrophic balance, Newtonian cooling and so on, this two-layer axisymmetric model can be solved analytically. Insights therefore can be gained on both the structure of the Hadley cell and its dependence on planetary parameters. The latitudinal extent derived from this model can be formulated as

$$\phi_H = \Big(\frac{5\Delta\theta_{rad} g H}{3\Omega^2 a^2 \theta_0}\Big)^{1/2}$$

in radians, where $\Delta\theta_{rad}$ is the radiative-equilibrium potential temperature difference between equator and the poles, Ω is the planetary rotation rate, θ_0 is the radiative-equilibrium potential temperature at the equator, a is the planetary radius, and H is the altitude of the upper layer.

As we can infer from this equation, the latitudinal extent of the Hadley cell is inversely proportional to the rotation rate and the planetary radius, and proportional to the square root of the prescribed equator-to-pole temperature difference. This is in good agreement with both our observations of other terrestrial planets in our Solar System and GCM simulations of the circulation under different rotation rate as shown in Figure 2.2. Although this axisymmetric model predicts reasonably well the structure of a Hadley cell given its simplicity, even better agreement can be achieved by taking the higher latitude eddy activities into account. Since the poleward extent of the Hadley cell represents the boundary beyond which eddies are dominating,

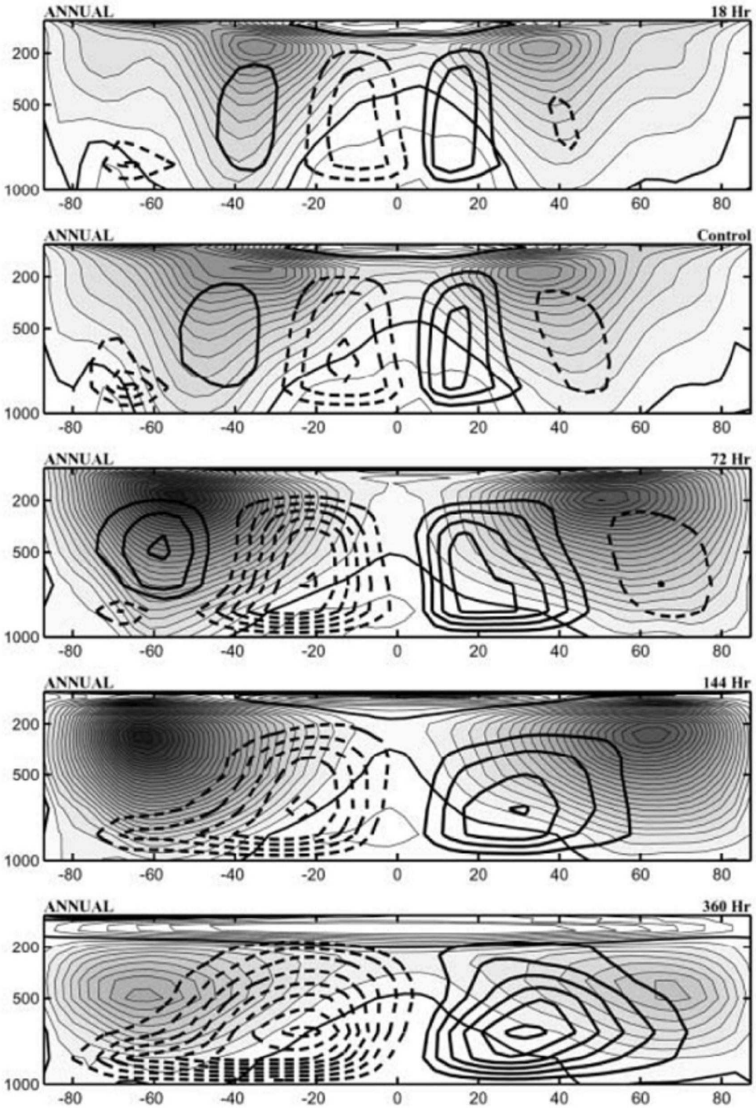

Figure 2.2: Zonal mean cross-sections of Hadley circulation at various rotation periods, from *Navarra and Boccaletti* [2002]

it is natural to expect that the interaction between eddies and Hadley cell is significant in the maintenance of the latitudinal extent of the latter. In the midlatitudes, zonal flow is generally accelerated by the baroclinic eddies. For a steady state to be possible, there must be an equatorward flow component such that the zonal Coriolis acceleration that arises is just enough to balance the eddy acceleration. This equatorward flow is counteracting the Hadley circulation, and the latitude where this flow totally offsets the Hadley flow defines the latitudinal boundary of the Hadley cell. Based on this idea, *Held* [2000] proposed another analytical result for the latitudinal extent of Hadley cell under the small angle approximation as the following:

$$\phi_H = \Big(\frac{gH\Delta\theta_v}{\Omega^2 a^2 \theta_0}\Big)^{1/4}$$

A comparison of the above stated two models with the GCM simulations is shown in Figure 2.3.

2.1.2 Baroclinic Waves and Eddies

The baroclinic region in mid- and high-latitudes is mainly characterised by meandering jets and transient baroclinic eddies(*Holton* [2004]). These eddies are highly important for the meridional transport of heat between the warm lower latitudes and the cold poles. Without these eddy activities excited by baroclinic instability, the extratropical atmosphere will relax to a radiative equilibrium which produces much greater equator-to-pole temperature difference. Therefore it would be helpful to figure out the efficiency of the eddy heat transport, which is helpful for our prediction of the temperature gradient on exoplanets based on limited observational data. The most obvious way to represent the effect of eddies in the circulation system is perhaps by running eddy–resolving GCMs which simulate the development and decay of each individual eddy. However, this straightforward method is not only computationally expensive but also physically unenlightening. A simplified parametrisation of eddy activities will be ideal for both numerical cost and our sensitivity studies on the parameter dependence of circulation regimes.

There are generally two approaches of simplification for the baroclinic eddy processes. One idea is to view the eddy activities as a restoring force to relax the mid-latitude atmosphere towards a neutrally stable baroclinic state, a mechanism known as baroclinic adjustment (*Stone* [1978]). This concept, as an analogy of convective adjustment, assumes that the eddy timescale is far smaller than the radiative timescale, thus making it possible that the eddies transport heat poleward at such a rate that they just

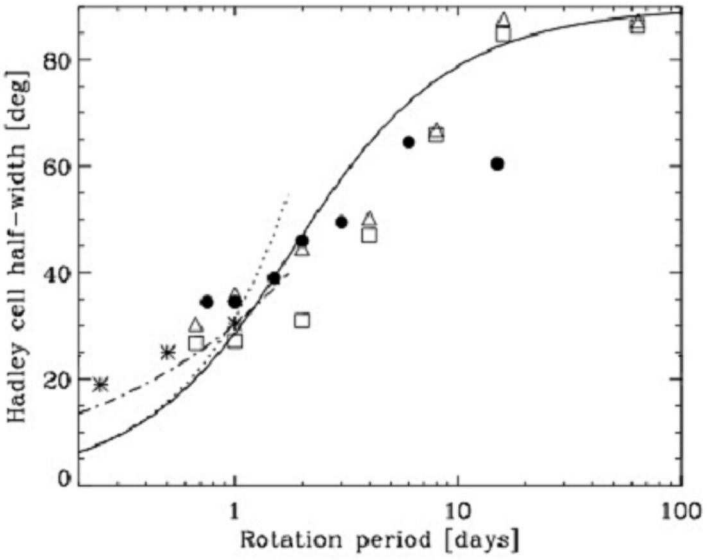

Figure 2.3: Comparison of the dependence of Hadley cell extent on rotation rate by different models and theories. Solid curve represents the complete theory of *Held and Hou* [1980], dotted curve the small-angle approximation of the *Held and Hou* [1980] theory, and the dash-dotted curve the *Held* [2000] theory. After *Showman et al.* [2010].

maintain the baroclinic atmosphere in a neutrally stable state. It predicts a critical slope of isentropes in a two-layer atmosphere around H/a, which fits surprisingly well with the observed value in the real atmosphere. However, when moving to a multi–layer atmosphere, the critical slope of isentropes will decrease as the number of layers increases. For a vertically continuous model, the critical slope goes to zero, indicating that the baroclinic zone can have any horizontal temperature difference smaller than that determined by the critical slope of H/a. This is because for small isentrope slope, baroclinic activities are weak and thus not playing a significant role in shaping the mean state atmospheric structure. Therefore in the real atmosphere, it is possible that baroclinic turbulence can only relax the isentrope slope to a value around H/a as we observed.

The other simplification method is to view the mid- and high latitude eddy activities as a kind of diffusive process(*Held* [1999]). It can be formulated as the following:

$$c\frac{\partial T}{\partial t} = \nabla \cdot (cD\nabla T) + S(\phi) - I$$

where c is the heat capacity of the atmosphere, T is the surface temperature, D is the diffusivity characterising the baroclinic eddy activities. $S(\phi)$ is the absorbed the stellar radiation as a function of latitude ϕ. I is the thermal radiation emitted by the atmosphere.

By simply parametrising the term I as $I = A + BT$ and $S(\phi)$ as a constant term plus a term proportional to the second Legendre Polynomial $P_2(\cos(\phi))$, a steady state solution of the equator–to–pole temperature difference can be obtained (*Held* [1999]) as

$$\Delta T_{EP} = \frac{\Delta T_{rad}}{1 + 6\frac{cD}{Ba^2}}$$

where a is the planetary radius and ΔT_{rad} is the pre–determined equator-to-pole temperature difference at radiative equilibrium.

Thus the determination of the temperature difference depends on the value of the eddy diffusivity D. In most of the Earth climate models, this parameter is determined by tuning it so that the simulated climate structure fits well with what we observed. But for the purpose of simulating other planets, especially those exoplanets where data concerning the climatic conditions is rarely available, we must find out the dependence of eddy diffusivity on planetary parameters which can be obtained through current observational techniques. A series of parametrisation of the diffusivity has

Scheme	L_{eddy}	D
Stone(1972)	L_D	$\frac{H^2 N g}{f^2 \theta_0} \frac{\partial \overline{\theta}}{\partial y}$
Green(1970)	L_{zone}	$L_{zone}^2 \frac{g}{N \theta_0} \frac{\partial \overline{\theta}}{\partial y}$
Held and Larichev(1996)	L_β	$\frac{g^3}{N^3 \beta^2 \theta_0^3} \left(\frac{\partial \overline{\theta}}{\partial y} \right)^3$
Barry et al.(2002)	L_β	$\left(\frac{e a \dot{q}_{net}}{\theta_0} \frac{\partial \overline{\theta}}{\partial y} \right)^{3/5} \left(\frac{2}{\beta} \right)^{4/5}$

Table 2.1: Baroclinic eddy diffusivity parametrisation schemes, after *Showman et al.* [2010].

been proposed by *Stone* [1972], *Green* [1970], *Held and Larichev* [1996], and *Barry et al.* [2002], as shown in Table 2.1. Numerical experiments are needed to test the validity of these different schemes.

2.2 Earth and Mars

As our neighbour and one of the most frequently explored planets within our Solar System, Mars shares a lot of atmospheric circulation features in common with the Earth. Both the Hadley cells and the baroclinic zones are observed on this red desert planet. And its similar rotation rate with the Earth determines most of these similarities in their circulation regimes.

As we can see from Figure 2.4, the Martian annual–mean circulation looks quite like that of the Earth, with two thermal-direct Hadley cells lying roughly anti-symmetrically along the equator, as well as two indirect cells at higher latititudes where baroclinic eddy activities are predominant and geostrophic balance stands. Sub-tropical jet streams can also be found on Mars albeit at higher latitudes than those on the Earth. The temperature field is featured by an equatorial warm core gradually cooling towards the poles within the troposphere, with more complicated latitudinal variations in the middle and upper atmospheres.

It should be pointed out that seasonal variation of the Martian circulation is significantly greater than that of the Earth(see *Read and Lewis* [2004]). For most time of the year, especially during those solstice seasons, the circulation is dominated by a cross-equator global Hadley cell which transports heat and mass from one hemisphere to the other. And the surface wind pattern at those times is eastward wind at the winter hemisphere and westward wind at the summer hemisphere, just like the wind distribution of Earth's middle atmosphere. There is a short time around the solstice

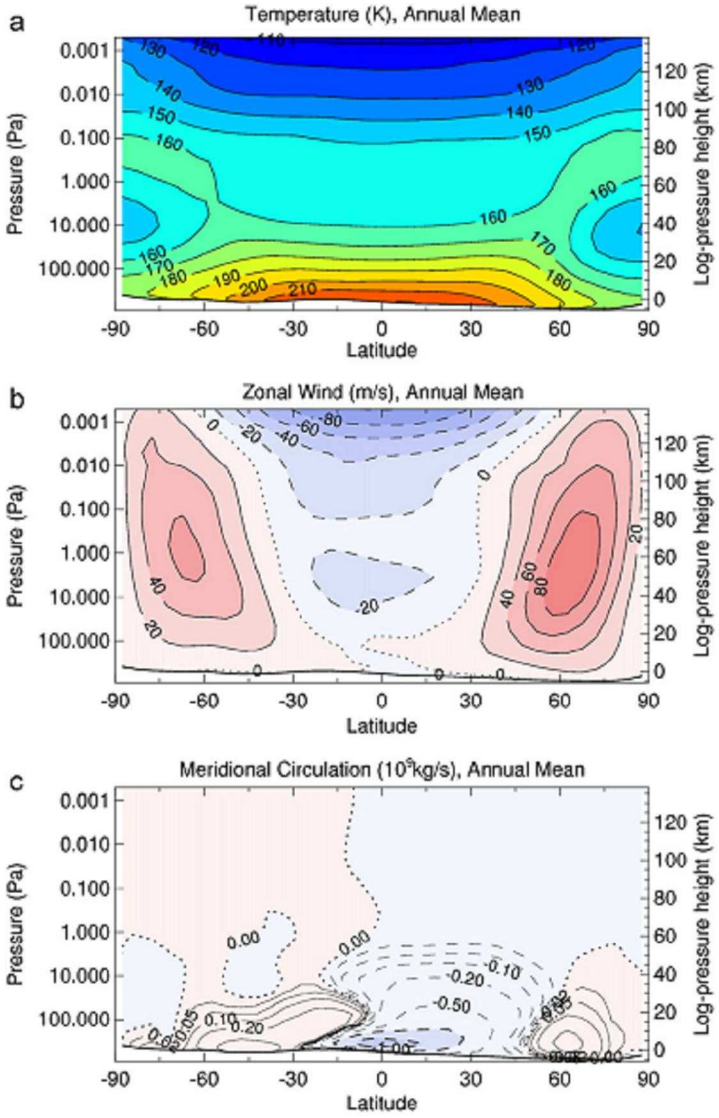

Figure 2.4: The zonal mean climatological field of Mars, after *Lewis et al.* [1999])

when the summer pole temperature is even larger than the equator. This greater extent of seasonal variation is mostly because of the small thermal inertia of the Martian climate system (thin atmosphere and lack of ocean) as well as its larger obliquity. In spite of these differences, the circulation patterns of Mars and the Earth are in most respects similar with each other, sharing a series of features of rapidly rotating planets in common.

2.3 Venus and Titan

Venus and Titan are slowly rotating planets with very different circulation regimes to those of the Earth and Mars. GCM simulations(*Lee et al.* [2005], see Figure 2.5) show that the zonal–mean circulation of Venus is dominated by two hemispheric Hadley cells ranging from the equator to very high latitudes. This, together with the very large radiative time scale on these two planets, leads to a much smaller meridional temperature difference compared with the Earth and Mars. The most remarkable feature of the zonal wind field is the globally prograde upper level wind. This is different from the situation on Mars and the Earth where prograde wind is only discovered at extratropical regions while the equatorial atmosphere is dominated by deep eastward wind (except during the westerly phase of the QBO—Quasi-Biennial Oscillation). This excess of angular momentum, compared with the angular momentum air would have in co-rotation with the underlying solid body, is known as the 'super–rotation'(*Read* [1986]). This is a unique feature of the slowly rotating planets. The very fast wind speed on Venus and Titan compared with the underlying solid planets indicates that geostrophic balance is no longer valid. In fact, cyclostrophic balance (the balance between centrifugal force and the pressure gradient force) is believed to be the major constraint of the large scale dynamics on Venus and Titan.

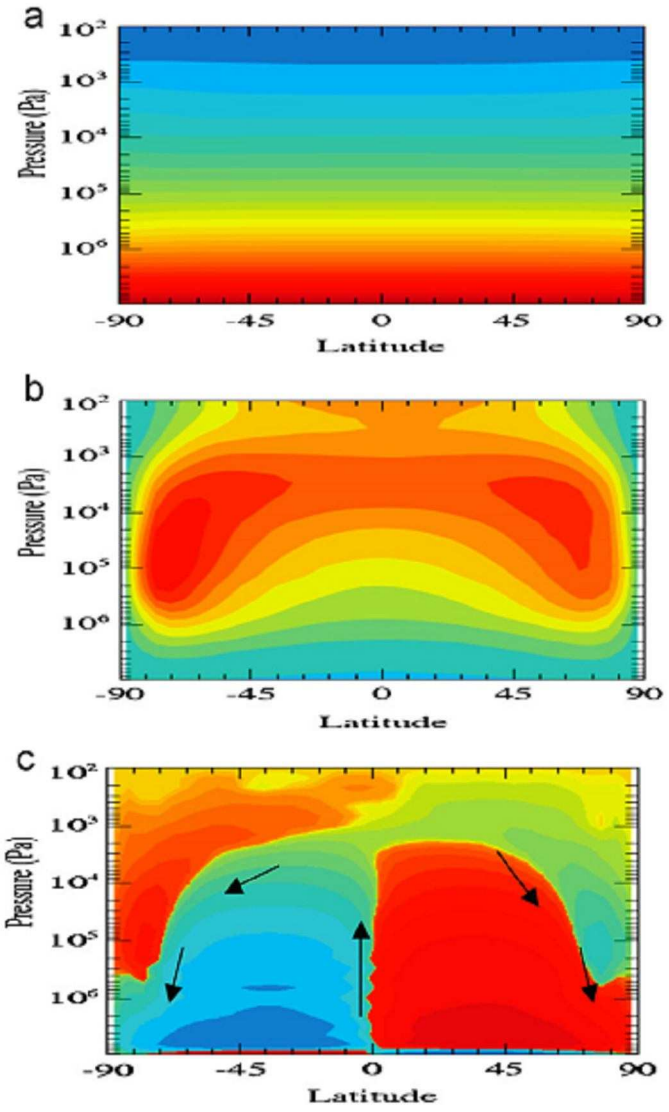

Figure 2.5: The zonal mean climatological field (GCM simulation). (a) Temperature, (b) Zonal wind, (c) Meridional mass streamfunction. After *Lee et al.* [2005].

Chapter 3

Parameter Dependence Study

As we can see from the previous chapter, the differences among the circulation regimes of the Earth, Mars, Venus and Titan can be ascribed to a variety of planetary parameters among which rotation rate is a crucial one. This naturally raises the question whether the characteristic features of the atmospheric circulation structure (e.g. range of Hadley cell, number and intensity of jets, efficiency of the meridional heat transport and so on) can be quantitatively figured out by using only a finite set of parameters. The approach in most science disciplines for tackling this kind of problem is usually to run sensitivity tests or controlled experiments. In the study of geophysical fluid dynamics, there are basically two branches of historical efforts—laboratory experiments using rotating annulus(or tank) with fluid heated from the boundaries and numerical experiments usually in the form of 3D general circulation models.

3.1 Laboratory Experiments

3.1.1 Apparatus and Configuration

One of the most frequently used laboratory apparatus by dynamical meteorologists in the past decades to study geophysical fluid motions is the rotating annulus with differentially heated inner and outer boundaries, as shown in Figure 3.1. The fluid is horizontally confined by two coaxial cylinders, and the whole system rotates around the vertical axis of symmetry with angular velocity Ω. If the outer cylinder (corresponding to the plan-

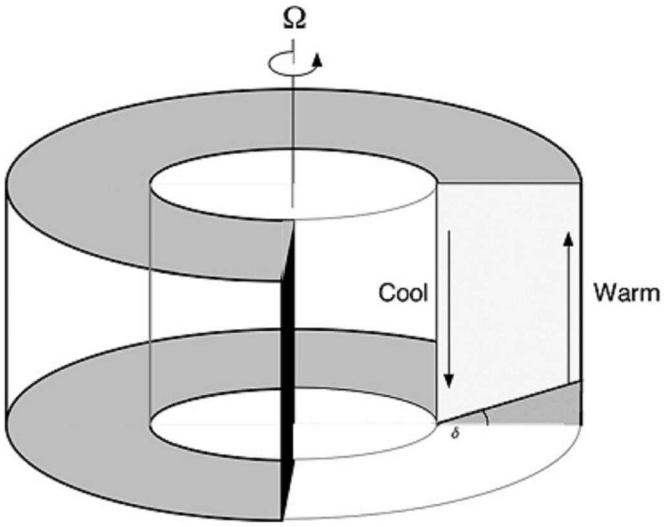

Figure 3.1: Schematic configuration of the rotating annulus experiment from Read(2010)

etary equator) is heated and the inner cylinder is cooled (corresponding to the planetary mid- and high-latitudes), this configuration roughly simulates the atmospheric circulations of terrestrial planets driven by differential heating. A conical slope can be added at the lower boundary to represent the equivalent β effect (*Hide and Mason* [1975]), leading to dispersive wave activity.

3.1.2 Non-dimensional Parameters and Flow Regimes

For the typical configuration of rotating annulus, at least two factors (the rotation speed as well as the exerted temperature difference between the inner and outer cylinder) can be tuned to conduct controlled experiments. But directly using the value of rotating rate or temperature difference to construct the parameter space in which circulation regimes are categorised might shed little light on our quantitative understanding of the behaviour of real atmosphere, since it could not get rid of the influence of the specific experimental configuration which is apparently far different from the planetary atmosphere in scale, density, etc. In order to avoid this influence of

individual experimental configuration and obtain generalisable results, we need to use non-dimensional parameters derived through applying dynamical similarity theory to fluids. Previous experiments have revealed that the most important non-dimensional parameters of the rotating annulus experiment are the Taylor number ($\mathcal{T}a$) and the thermal Rossby number($\mathcal{R}o$) (*Hide and Mason* [1975];*Hide* [1969]):

$$\mathcal{T}a = \frac{4\Omega^2 L^5}{\nu^2 D}$$

$$\mathcal{R}o \simeq \frac{U_T}{\Omega L} = \frac{g\alpha\Delta T\Delta D}{\Omega^2 L^2}$$

where L is the channel width, D is the depth, ν is the kinematic viscosity coefficient of the fluid and α is the volume expansion coefficient.

A review of Rhines' theory of geostrophic turbulence (*Rhines* [1975]) will provide us with several estimates of other interesting parameters like the Rhines scale:

$$L_R = \pi\Big(\frac{2U_{rms}}{\beta}\Big)^{1/2}$$

which is a characteristic length scale of the latitudinal range of eddies (either barotropic or baroclinic) on a β plane. By estimating the characteristic velocity scale U_{rms} with the thermal wind U_T in the annulus, and estimating β by

$$\beta = \frac{2\Omega\tan\delta}{D}$$

we can rewrite the Rhines length scale as:

$$L_R = \Big(\frac{g\alpha\Delta T D^2\pi^2}{\Omega^2 L\tan\delta}\Big)^{1/2}$$

This gives rise to another non-dimensional parameter: Rhines number $\mathcal{R}_h$ defined in the form of:

$$\mathcal{R}_h = \frac{L^2}{L_R^2} = \frac{\Omega^2 L^3\tan\delta}{g\alpha\Delta T D^2\pi^2}$$

It can be related to the thermal Rossby number $\mathcal{R}o$ as:

$$\mathcal{R}_h = \frac{L\tan\delta}{D\pi^2}\mathcal{R}o^{-1}$$

If the Rhines scale does not exceed the width of the annulus channel, the number of jets within the channel can be estimated using Rhines number as $N_J = \sqrt{\mathcal{R}_h}$ (*Bastin and Read* [1998]; *Sukoriansky et al.* [2007]).

Using thermal Rossby number and Taylor number to construct the 2-D parameter space (plane), we can map the occurence of the type of flow we observed in the experiments. The map we obtained by this method shows the parametric dependence of the flow pattern, and is known as the *regime diagram*. Figure 3.2 is the regime diagram from *Hide and Mason* [1975], showing results of a series of experiments under various rotation rate and exerted temperature difference.

In this regime diagram, isotherms are lines with a slope of 45° from the top left to the bottom right. Thick solid curves represent the transition boundaries of flow patterns. Therefore, increasing the rotation rate while holding the temperature difference between the outer and inner boundaries, the flow will transit from axisymmetric flow to steady or vacillating regular waves and finally to irregular and chaotic flows or even turbulence.

3.2 Numerical Experiments

The history of using numerical models to study the atmospheric behaviours is roughly as long as the laboratory experiments of rotating annulus (The first successful NWP was made by a team led by Jule Charney in 1950, using ENIAC). However, a majority of the previous efforts on numerical studies were focussed on the weather forecast with synoptic time scale as well as running highly comprehensive Earth-based GCMs to study the climate variability. Sensitivity tests and controlled expriments on various sets of parameters, on the other hand, have not been given much attention within the numerical modelling community. But a series of scattered numerical experiments taking a parametric approach were published in the last few decades, and some of them even came up with preliminary regime diagrams.

3.2.1 Non-dimensional Parameters

Since the atmosphere is essentially a rotating stratified fluid forced by differential heating, just like the fluid within the annulus, we expect that the thermal Rossby number and Taylor number also play significant roles in shaping the circulation regimes of the real atmosphere. However, due to the geometric difference between the cylindrical annulus and the spherical planetary atmosphere, the expressions might be different.

The numerical model thermal Rossby number is defined as the following:

$$\mathcal{R}o = \frac{R\Delta\theta_h}{\Omega^2 a^2}$$

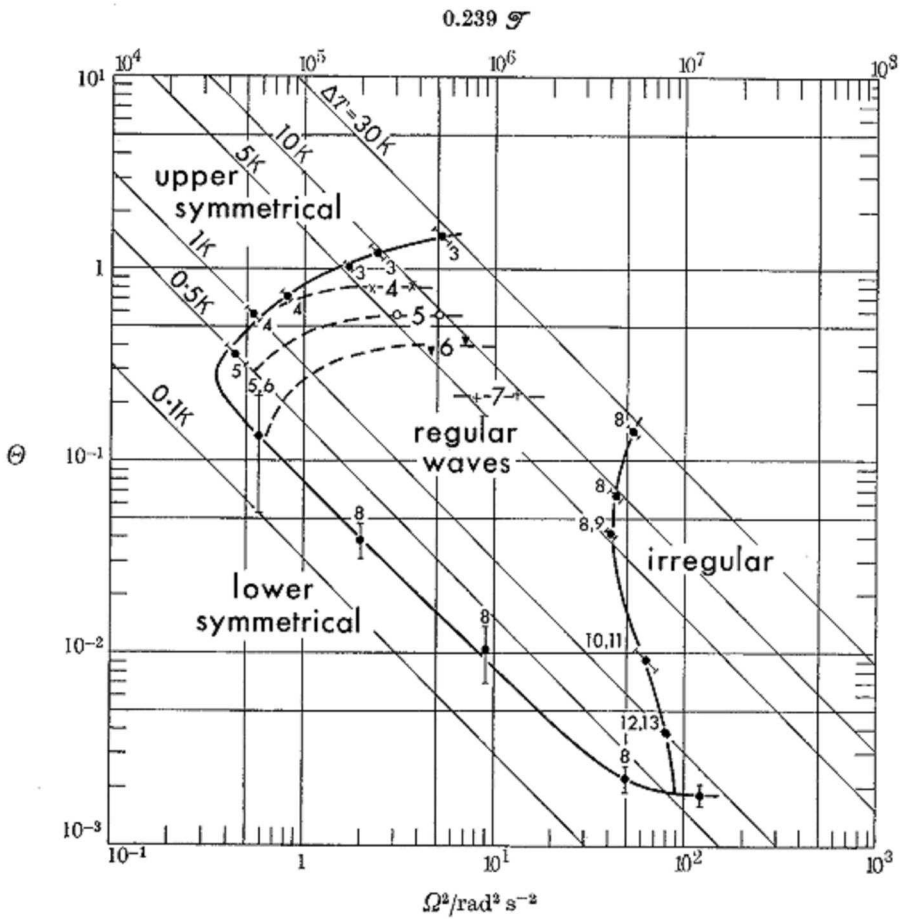

Figure 3.2: Regime diagram from *Hide and Mason* [1975]

Here the horizontal length scale L has been replaced by the planetary radius a, and the vertical scale H is replaced by the pressure scale height $H = RT_0/g$, where T_0 is the characteristic temperature and R is the specific gas constant. Note that the imposed temperature difference ΔT is replaced by the horizontal potential temperature difference $\Delta\theta_h$ which is not directly set and controlled by the experimenter, but rather an internal parameter partly determined by the heat transport effeciency of the model atmosphere.

Similarly, the Rhines length scale can be written as:

$$L_R \simeq \pi\Big(\frac{R\Delta\theta_h}{4\Omega^2}\Big)^{1/2}$$

and the corresponding Rhines number is formulated as:

$$\mathcal{R}_h = \frac{a^2}{L_R^2} \simeq \frac{4\Omega^2 a^2}{\pi^2 R\Delta\theta_h} = \frac{4}{\pi^2}\mathcal{R}o^{-1}$$

Note that here the Rhines number is inversely proportional to the thermal Rossby number, without dependence on the boundary slope δ, which is different from the case in rotating annulus.

Rhines' theory on the structure of zonal flows and eddies states that the latitudinal variation of f (i.e. β effect) leads to anisotropy of eddies, causing elongation in the east-west direction, thus giving rise to the zonal banded structure. The characteristic length scale at which this kind of flow reorganisation happens is given by the Rhines scale. Thus if the Rhines scale is smaller than the planetary domain, it will be possible to observe banded structures in the global circulation pattern. Figure 3.3 Shows the results of a 2-D non-divergent numerical simulation of eddy growth on a sphere at different rotating rates. It can be clearly seen that multiple zonal jets appear as the planet rotates faster (fast rotation rate corresponds to small Rhines scale), which fits well with Rhines' theory.

For the atmospheric circulation, Taylor number is no longer a crucial parameter since the dissipation within the atmosphere is mainly due to eddies and friction at surface, while the molecular viscosity has only a marginal effect. Instead, frictional and radiative damping parameters $\mathcal{F}_r$ and F_f are defined as the analogues to $\mathcal{T}_a$ in the laboratory rotating annulus:

$$\mathcal{F}_r = 4\Omega^2\tau_r^2$$

$$\mathcal{F}_f = 4\Omega^2\tau_r^2$$

where the τ_r and τ_f are characteristic radiative and frictional timescales respectively.

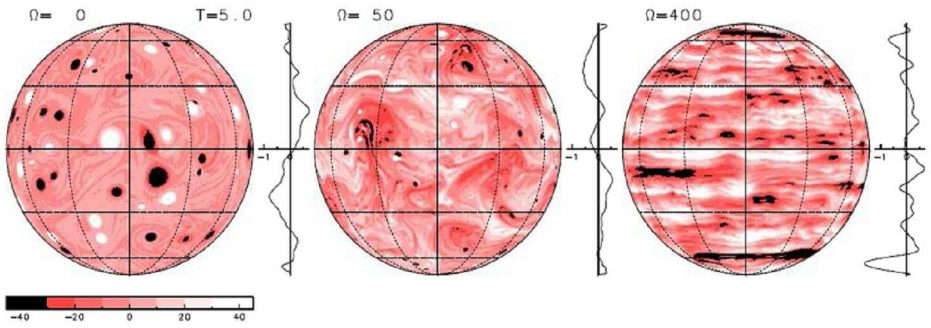

Figure 3.3: Multiple jets formation as the rotation rate increases, after *Yoden et al.* [1999],*Hayashi et al.* [2000]

3.2.2 Circulation Regimes in Model Simulation

There has been continuous efforts of conducting numerical experiments on the sensitivity of circulation regimes to planetary parameters during the past decades, although based on a variety of motivations, as we mentioned in Chapter 1. One of the early fruitful attempts is that done by *Geisler et al.* [1983] focussing on the dependence of circulation regimes on the rotating rate. They used a simplified GCM adapted from CCMZ(the Community Climate Model, Version Zero), which is a spectral model with nine vertical sigma levels. The hydrological cycle, radiation and topography were removed from the model, and the physics was reduced to Newtonian cooling and constant surface drag coefficient of 0.004. By varying both the rotation rate and the imposed equator-to-pole temperature difference, they finally yielded a regime diagram with thermal Rossby number as the ordinate and the inverse square of Ekman number (which is viewed as an equivalent of the Taylor number in the rotating annulus) as the abscissa, as shown in Figure 3.4. As we can see from this regime diagram, the boundary between the axisymmetric flow in which no wave activities are detected and the region where flows are dominated by baroclinic waves stretches from the top left to the bottom right corner of the diagram. What is different from the laboratory annulus diagram is that there is no upper symmetric region in their regime diagram, which is possibly due to the difference of geometry between rotating annulus and rotating spherical shell. Above this

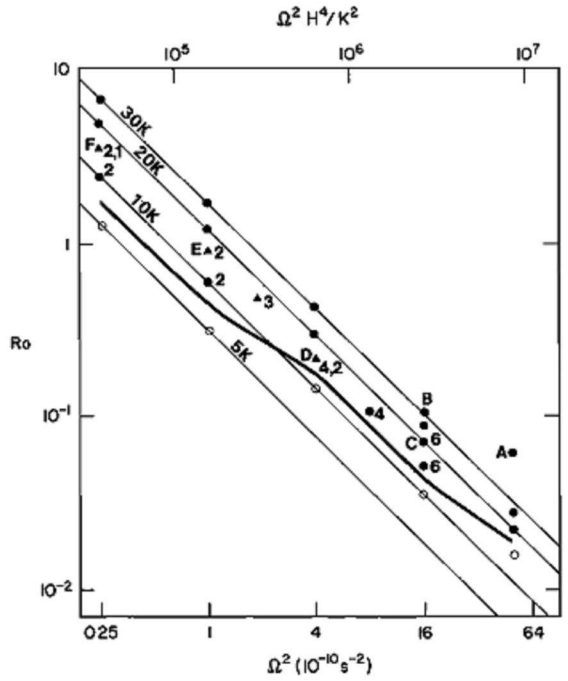

Figure 3.4: Regime diagram from *Geisler et al.* [1983]

boundary, three different flow patterns are identified: steady wave with single wavenumber and steady amplitude (denoted by black solid dots with dominating wavenumber labelled at its right side); wave with wavenumber one or two and oscillating amplitudes (denoted by black solid triangles with dominating wavenumber labelled at its right side); irregular wave with wavenumber greater than two and changing amplitudes (denoted by just black solid dots with no wavenumber labelled). Similar to the laboratory regime diagram, runs with constant temperature difference are straight lines from the top left to the bottom right with a slope angle of 45°. Point A is the terrestrial point with $\Delta T = 60K, \Omega = 7 \times 10^{-5} s^{-1}$. Most of the runs in this regime diagram are with rotation rate smaller than the Earth's and temperature difference smaller than $60K$. A systematic investigation of the issue, however, should include configurations with higher rotation rate and larger temperature difference.

The most comprehensive study on the sensitivity of Earth-like planets to defining planetary parameters so far is probably that done by Williams in late 1980s (*Williams* [1988a]; *Williams* [1988b]). In his two papers, Williams showed a series of results by changing rotation rate, obliquity, etc. for both dry atmosphere and moist atmosphere. Suprisingly, however, he did not came up with a regime diagram to quantitatively encompass all these results. He even didn't try to represent the effects of these planetary parameters into non-dimensionalised parameters. Figure 3.5 and Figure 3.6 shows the latitude-height cross-sections of zonal mean zonal wind and temperature under different rotation rates ranging from 8Ω to $1/16\Omega$. Clear trends can be seen in these plots. As the rotation rate goes slower, the zonal jet drifts poleward and becomes intensified, and the horizontal temperature gradient is reduced due to the expansion of the overturning Hadley circulation. As the rotation rate goes faster, multiple zonal jets appear and the temperature field develops a kind of staircase-like features which can be ascribed to the existence of alternating eastward-westward baroclinic zones.

Other studies have revealed similar trends in circulation indexes while varying the Earth's rotation rate in a GCM(see *Navarra and Boccaletti* [2002], *Del Genio and Suozzo* [1987]). The Hadley cell basically expands poleward and strengthens if you decrease the rotation rate. Multiple jets, like what we observed on Jupiter and Saturn, can be found if we increase the rotation rate.

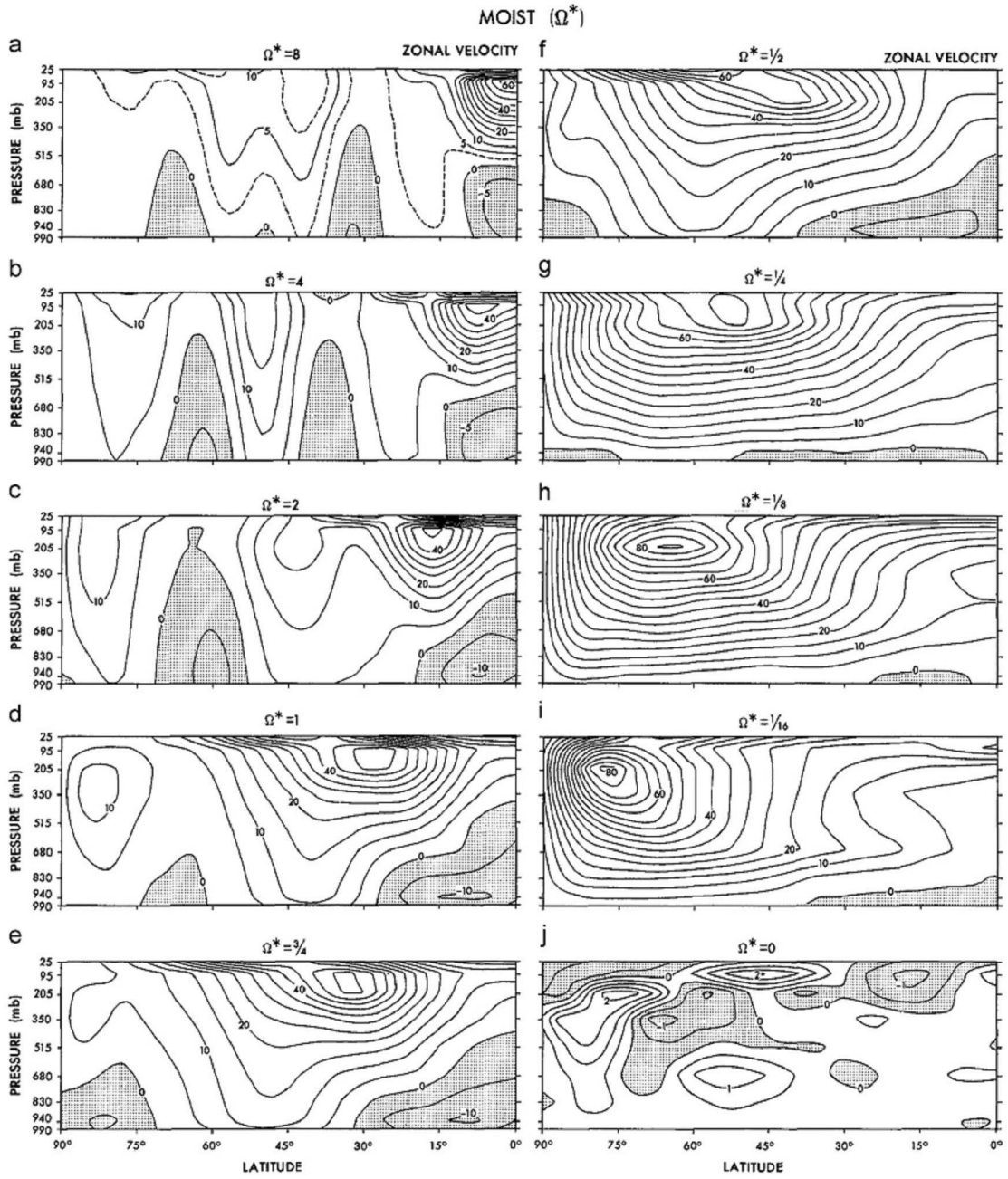

Figure 3.5: Zonal mean cross–sections of zonal wind and temperature for rotation rate Ω^* from 8Ω to $1/16\Omega$.

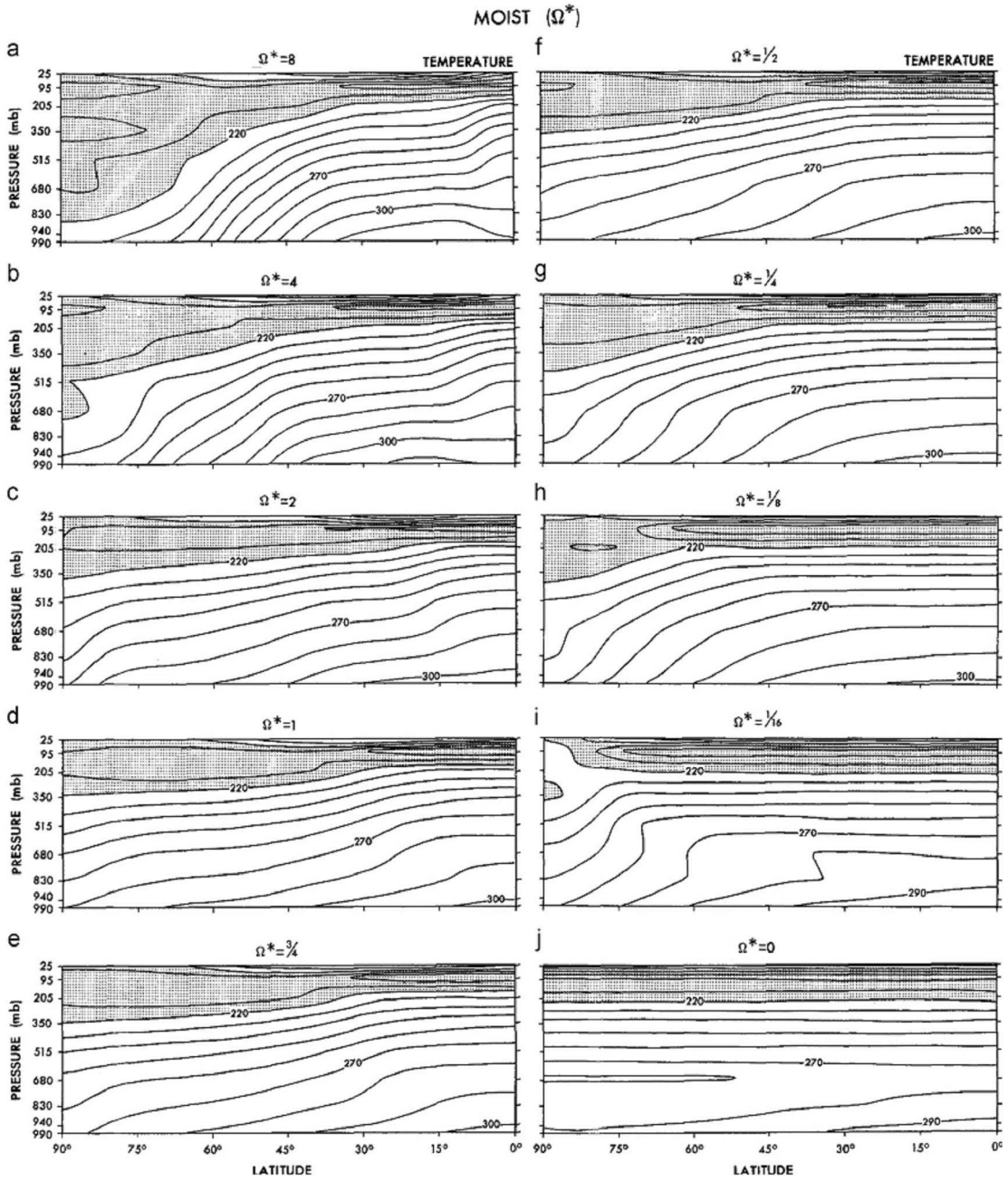

Figure 3.6: Same as Figure 3.5, but the plotted variable is the zonal mean temperature

Chapter 4

PUMA

4.1 Model description and dynamics

PUMA(Portable University Model of the Atmosphere), is a simplified GCM developed by the Meteorological Institute, University of Hamburg. It consists of a spectral dynamical core based on the SGCM (Simple Global Circulation Model) described by *Hoskins and Simmons* [1975], plus several highly simplified physical processes. Newtonian cooling scheme is used to represent the radiative heating and cooling effect, and surface frictional effect is assumed to bear the form of linear Rayleigh friction. Hydrology, cloud and aerosol physics, as well as biological effect are not taken into account. Developed with the aim of training young scientists and students, PUMA has a friendly Graphical Model Starter (MOST) and Graphical User Interface (GUI) which enable the user to conveniently configure and run the model (as shown in Figure 4.1 and Figure 4.2).

4.1.1 Dynamical core

The dynamical core of the model is based on the primitive equations describing the conservation of momentum, mass and energy. They can be written in the dimensionless form as the following:

Conservation of momentum

Vorticity equation

$$\frac{\partial(\zeta + f)}{\partial t} = \frac{1}{(1-\mu^2)}\frac{\partial F_v}{\partial \lambda} - \frac{\partial F_u}{\partial \mu} + P_\zeta$$

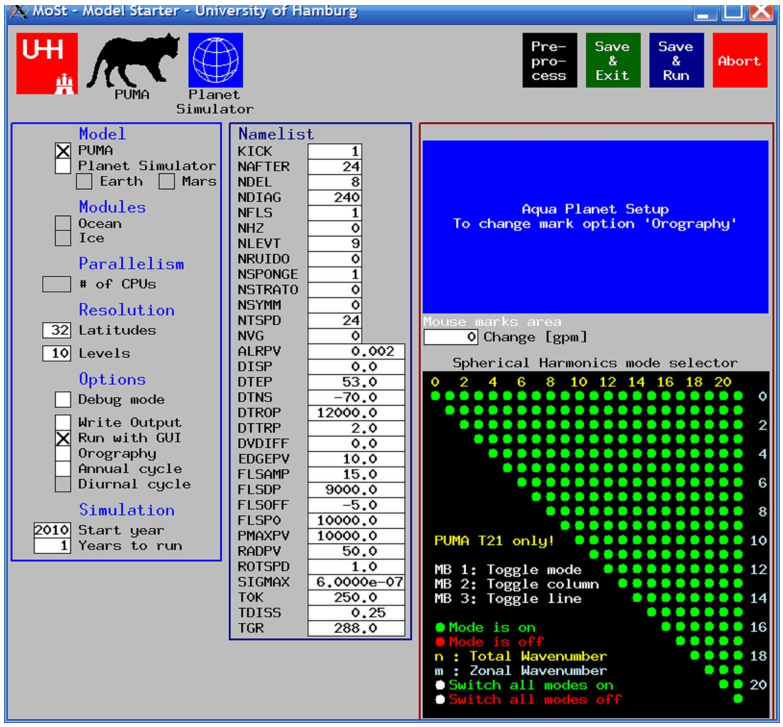

Figure 4.1: The Model Starter (MOST) of PUMA

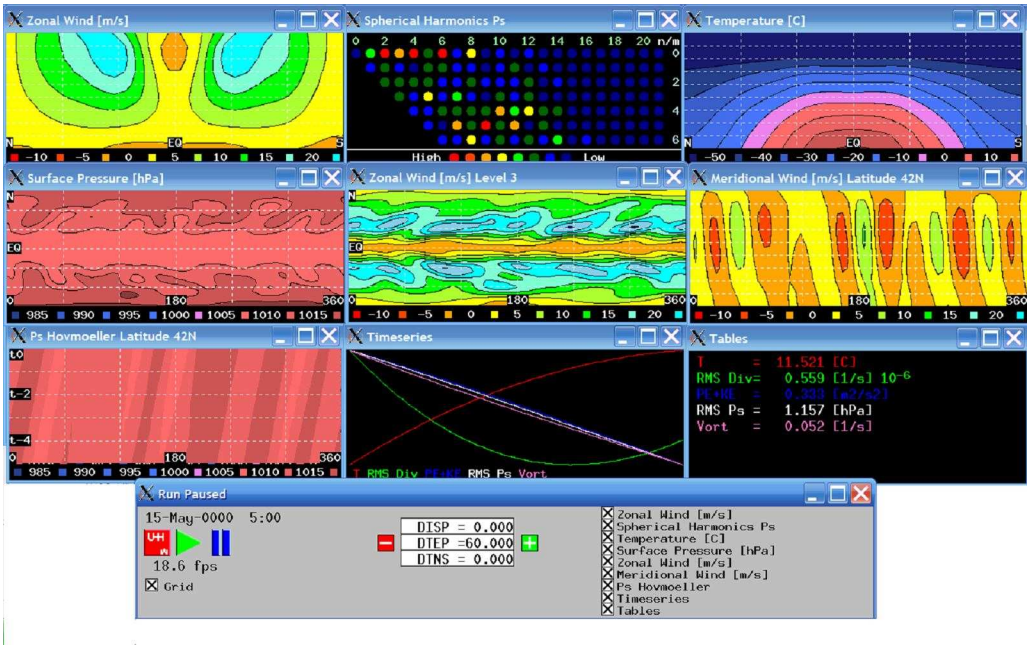

Figure 4.2: The Graphical User Interface (GUI) of PUMA

Divergence equation

$$\frac{\partial D}{\partial t} = \frac{1}{(1-\mu^2)}\frac{\partial F_u}{\partial \lambda} + \frac{\partial F_v}{\partial \mu} - \nabla^2\left(\frac{U^2+V^2}{2(1-\mu^2)} + \Phi + T_0 \ln p_s\right) + P_D$$

Hydrostatic equilibrium

$$\frac{\partial \Phi}{\partial \ln \sigma} = -T$$

Conservation of mass

Continuity equation

$$\frac{\partial \ln p_s}{\partial t} = -\int_0^1 A \mathrm{d}\sigma$$

Conservation of energy

First law of thermodynamics

$$\frac{\partial T'}{\partial t} = -\frac{1}{(1-\mu^2)}\frac{\partial (UT')}{\partial \lambda} - \frac{\partial (VT')}{\partial \mu} + DT' - \dot{\sigma}\frac{\partial T}{\partial \sigma} + \kappa\frac{T}{p}\omega + \frac{J}{c_p} + P_T,$$

where

$$F_u = V(\zeta + f) - \dot{\sigma}\frac{\partial U}{\partial \sigma} - T'\frac{\partial \ln p_s}{\partial \mu}$$

$$F_v = -U(\zeta + f) - \dot{\sigma}\frac{\partial V}{\partial \sigma} - T'(1-\mu^2)\frac{\partial \ln p_s}{\partial \mu}$$

$$A = D + \overrightarrow{V} \cdot \nabla \ln p_s$$

$$U = u\cos\phi, V = v\cos\phi$$

and the physical meaning of the variables are:

T	temperature
T_0	reference temperature
$T' = T - T_0$	temperature deviation
ζ	relative vorticity
D	Divergence
p_s	surface pressure
p	pressure
Φ	geopotential
t	time
λ, ϕ	longitude, latitude
μ	$\sin\phi$
σ	p/p_s Sigma coordinate in vertical direction
$\dot{\sigma} = d\sigma/dt$	vertical velocity in σ coordinate system
$\omega = dp/dt$	vertical velocity in pressure coordinate system
u, v	zonal and meridional velocity component
$\overrightarrow{V}$	(u, v)
$f = 2\Omega\sin\phi$	Coriolis parameter
J	diabatic heating rate
c_p	specific heat capacity of dry air at constant pressure
κ	R/c_p where R is the specific gas constant

Variables within these equations are nondimensionalised by scaling. Vorticity and divergence are scaled by Ω, pressure p and p_s by the mean surface pressure $1011hPa$, temperature T and T_0 by $a^2\Omega^2/R$ (here a is the radius of the Earth), geopotential Φ by $a^2\Omega^2/g$, and time t by Ω^{-1}. Triangular truncation is used for the horizontal spectral calculation, and σ–coordinate is used for the vertical discretisation.

4.1.2 Parameterisation of physical processes

Friction

Dissipation terms in the vorticity and divergence equations are parameterised as Rayleigh friction:

$$P_\zeta = \frac{\zeta}{\tau_F} + H_\zeta$$

$$P_D = \frac{D}{\tau_F} + H_D,$$

where τ_F is the characteristic timescale of dissipation, H_ζ and H_D are the hyperdiffusion terms.

Diabatic Heating

Diabatic heating of the atmosphere is simply parameterised by Newtonian cooling:

$$\frac{J}{c_p} + P_T = \frac{T_R - T}{\tau_R} + H_T,$$

where τ_R is the characteristic timescale for the temperature field to relax towards the prescribed restoration temperature field, H_T is the hyperdiffusion term. The restoration temperature field is defined as a function of latitude and height:

$$T_R(\phi, \sigma) = T_R(\sigma) + f(\sigma) T_R(\phi),$$

in which

$$T_R(\sigma) = (T_R)_{tp} + \sqrt{\Big[\frac{L}{2}(z_{tp} - z(\sigma))\Big]^2 + S^2} + \frac{L}{2}\Big(z_{tp} - z(\sigma)\Big),$$

where $(T_R)_{tp} = (T_R)_{grd} - L z_{tp}$ is the restoration temperature at the tropopause, L the vertical lapse rate, z_{tp} the global constant height of the tropopause, $(T_R)_{grd}$ the restoration temperature at the ground. S acts as a smoothing term at the tropopause.

The meridional variation of the restoration temperature field is formulated by

$$T_R(\phi) = (\Delta T_R)_{NS} \frac{\sin\phi}{2} - (\Delta T_R)_{EP}\Big(\sin^2\phi - \frac{1}{3}\Big),$$

where $(\Delta T_R)_{EP}$ is the prescribed constant restoration temperature difference between the equator and the poles, $(\Delta T_R)_{NS}$ is the variable part of the

meridional temperature gradient which changes with time to simulate the annual cycle.

The meridional variation is shaped by function $f(\sigma)$ so that the variation vanishes at the isothermal tropopause:

$$f(\sigma) = \sin\Big(\frac{\pi}{2}(\frac{\sigma - \sigma_{tp}}{1 - \sigma_{tp}})\Big)$$

while $\sigma \geq \sigma_{tp}$. If $\sigma < \sigma_{tp}$, then $f(\sigma) = 0$.

Hyperdiffusion

Hyperdiffusion terms H_ζ, H_D and H_T are needed in order to represent the effect of subgrid horizontal mixing and energy dissipation. For an arbitrary model variable Q (Q might be ζ, D or T), we have the hyperdiffusion in the following form:

$$H = -(-1)^h K \nabla^{2h} Q(\lambda, \mu, t)$$

or, in spectral form,

$$H = -(-1)^h K \nabla^{2h} \sum_\gamma Q_\gamma(t) Y_\gamma(\lambda, \mu),$$

where $\gamma = (n, m)$ designates the spectral modes($n = 1, 2, 3, ...$:total wave number; $m = 0, \pm 1, \pm 2, \pm 3, ...$: zonal wave number, with$|m| \leq n$ representing triangular trunction), and Y_γ are the spherical harmonics.

Using the condition that the spectral modes with $n = n_T$ are damped with a prescribed time scale τ_H:

$$H_\gamma = -\frac{1}{\tau_H} Q_\gamma(t) Y_\gamma(\lambda, \mu) \quad if$$

n=n$_T$,

we have

$$K = \frac{1}{\tau_H}\Big(\frac{a^2}{n_T(n_T + 1)}\Big)^h,$$

where n_T is the trunction of the total wave number(e.g. T21 corresponds to $n_T = 21$).

Thus,

$$H_\gamma = -\frac{1}{\tau_H}\Big(\frac{n(n+1)}{n_T(n_T + 1)}\Big)^h Q_\gamma(t) Y_\gamma(\lambda, \mu).$$

A standard value of h is set to 4, and the diffusion time scale is usually set to $\tau_H = 1/4d$.

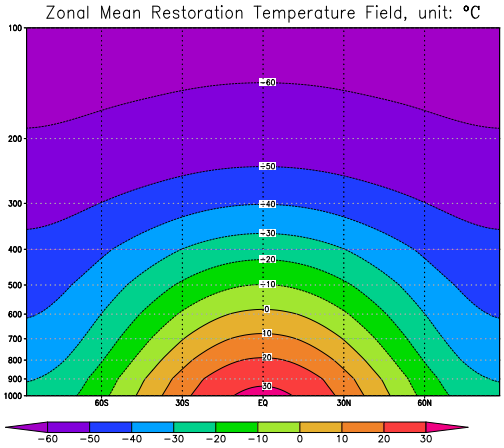

Figure 4.3: Restoration temperature field with $60K$ equator-to-pole temperature difference

4.2 Experiment design and configuration

In this project, PUMA is used to study the behaviour of a prototype atmosphere (albeit the atmospheric composition, planetary gravity and radius are still set to terrestrial values...). Due to the simplicity of the physical processes it includes, PUMA can be viewed as an equation solver of the non–linear primitive equation set. An aqua planet setting is used so that the topographical effects caused by the distribution of continents and oceans that are peculiar to the Earth can be avoided. Annual cycle as well as diurnal cycle are turned off and a fixed meridionally symmetric restoration temperature field is applied (a perpetual equinoctial thermal forcing). 10 σ levels $(0.1, 0.2, 0.3, 0.4, 0.5, 0.6, 0.7, 0.8, 0.9, 1.0)$ are set in the vertical direction. A constant vertical eddy-diffusion coefficient $K = 2m^2s^{-1}$ is used while the horizontal eddy-diffusion is set to zero. The simulation time is 20 model years in each run to ensure the atmosphere can manage to spin up to an equilibrium state.

We ran the model with various rotation rates ranging from 8Ω(8 times the rotation rate of the Earth) to $1/16\Omega$(1/16 times the rotation rate of the Earth), prescribed equator-to-pole restoration temperature difference of $120K$, $60K$(which is roughly the observed mean value on the Earth), and $30K$. The restoration temperature field with $60K$equator-to-pole temperature difference is shown in Figure 4.3. Resolution of T127 is used for 8Ω to 2Ω runs, while T21 is used for 1Ω to $1/16\Omega$ runs. Both the radiative

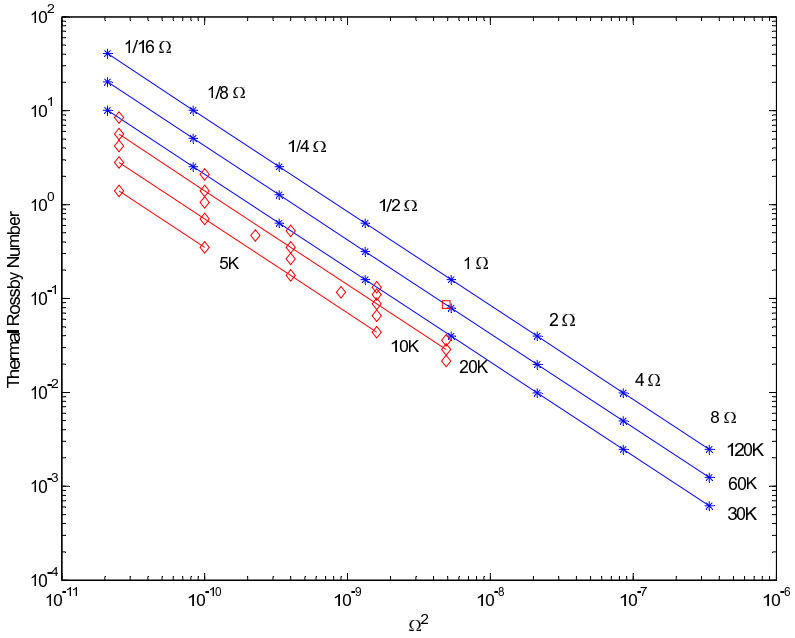

Figure 4.4: Simulation runs plotted in the parameter space. Red boxes and lines represent the experiments of *Geisler et al.* [1983]

relaxation timescale τ_r and the frictional timescale τ_f are set to the same absolute values among the runs of different rotation rate. The radiative timescale is 30.0, 30.0, 30.0, 29.0, 25.3, 21.3, 16.9, 12.3, 7.5, 2.5 Earth days from the top level to the bottom. The frictional timescale is 0.6 Earth days at the lowest level, 1.6 Earth days at the second lowest and ∞ at all the above levels (no friction within the free atmosphere). The simulations we conducted can be mapped in the parameter space constructed by thermal Rossby number and Ω^2 (which can be viewed as a substitute for either $\mathcal{F}_f$ or $\mathcal{F}_r$ since the radiative/frictional timescales are set to the same absolute value throughout the experiments) as shown in Figure 4.4.

Chapter 5

Diagnostic Results

In this chapter we will systematically investigate the diagnostic results of the circulation patterns obtained in our numerical experiments. By looking at the zonal mean field as well as the transient wavy structure, we discover a variety of regimes for different values of planetary parameters. Comparisons between these diagnostics and the planetary circulation on Solar System planets show very similar trends for the dependence of circulation regime on rotaion rate. At the end of this chapter, an interesting experiment of changing the planetary radius while holding the rotating rate to 1Ω is discussed.

5.1 Spin-up

PUMA runs from an initial state of motionless atmosphere (by setting the divergence and vorticity to zero). The initial temperature field is horizontally constant, while the vertical distribution is adopted from the restoration temperature field, which is usually stably stratified. A random white noise perturbation is applied to the initial surface pressure field. The spin-up phase refers to the time interval from the initial start point to the time when the atmosphere reaches a state of (near) equilibrium. The initial globally integrated kinetic energy is zero. During the spin-up phase, the kinetic energy of the system grows rapidly with time through the development of the thermal driven atmospheric circulation, which constantly converts available potential energy to kinetic energy. We use the globally averaged kinetic energy as the index of the spin-up phase. Once the globally averaged kinetic energy reaches a more or less constant level with little variation, we assume that the atmosphere has reached the equilibrium state.

As we can see from Figure 5.1, the global atmosphere spins up to an

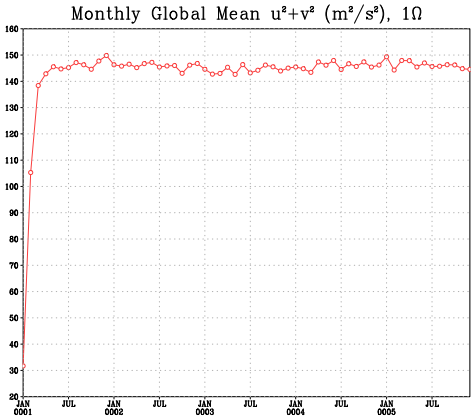

Figure 5.1: Spin-up phase of 1Ω run

equilibrium state fairly quickly (within two years) at the terrestrial rotation rate. For other representative values of rotation rate, the time might be a bit longer, as shown in the figures below.

In this project, all the simulations are ran for 20 model years from the initial motionless atmosphere to ensure that the global atmosphere can spin up to the equilibrium state. The mean values of meteorological variables over the last 12 months of the simulation are used while performing temporal average.

5.2 Zonal mean field diagnostics

Since the incoming solar radiation which serves as the ultimate energy source of atmospheric circulation generally varies most in the meridional direction, the large-scale motion of the atmosphere has greater variations in the meridional direction than in the zonal direction, especially when averaging over a long time period (more than one year, for example). Thus analysis of the zonal average of the meteorological variables takes a significant role in the study of atmospheric circulation. In fact, for some early meteorologists before the 20th century, the concept of general circulation refers exactly to these zonal mean diagnostics(*James* [1994]). The zonal mean zonal wind (U) for the runs 8Ω to 1/16Ω is shown in Figure 5.4 as below.

As we can see from this figure, the subtropical jet stream moves to higher latitude as the rotation rate decreases, which is consistent with the prediction from the symmetric Hadley cell theory (see *Held and Hou* [1980]). The

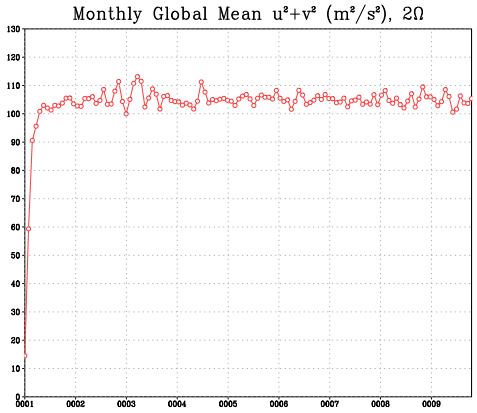

Figure 5.2: Spin-up phase of 2Ω runs

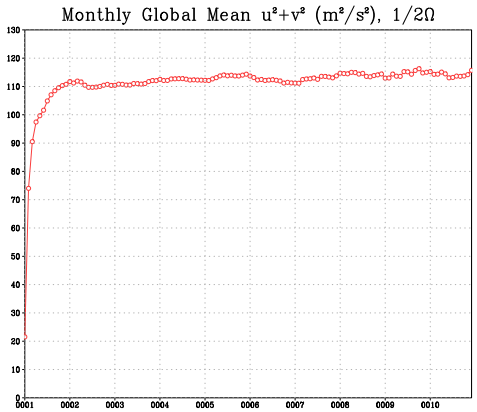

Figure 5.3: Spin-up phase of 1/2Ω runs

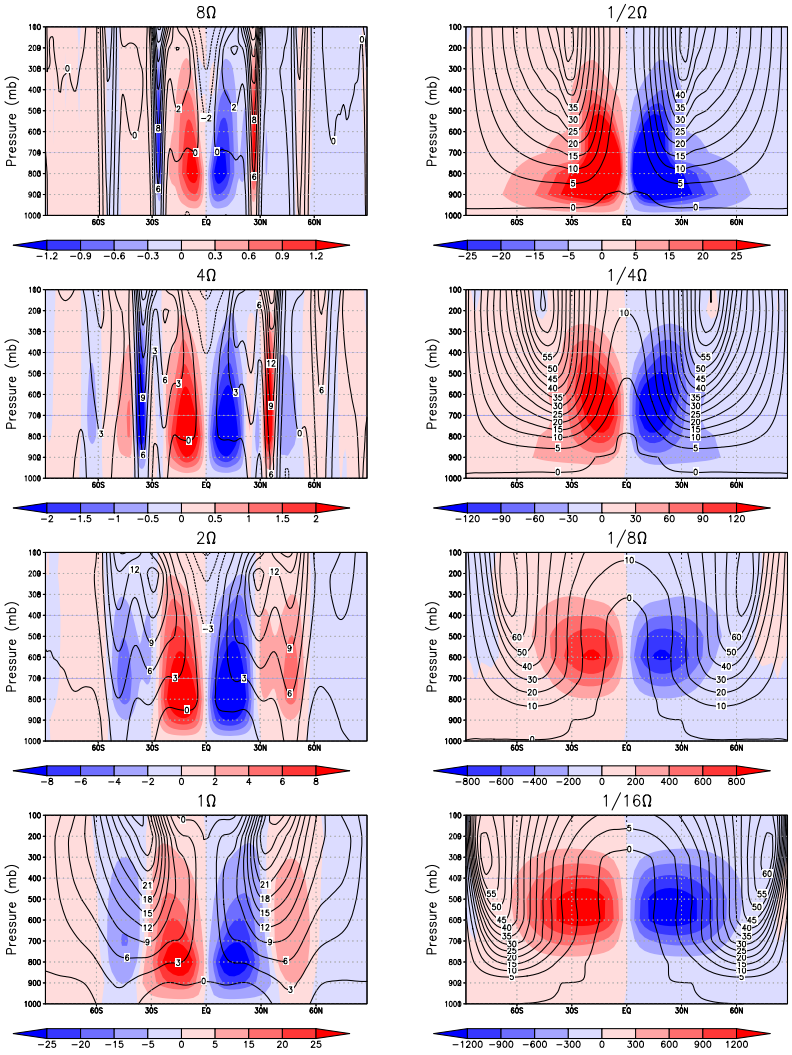

Figure 5.4: Zonal mean zonal wind and the meridional mass streamfunction

intensity of the jet stream grows stronger as the rotation rate decreases, but does not go monotonically with the rotation rate. For the $1/16\Omega$ run, the jet is actually weaker than that in the $1/8\Omega$ run. In principle, there are two competing factors determining the intensity of the subtropical jet stream as the rotation rate decreases. The jet stream reaches higher latitude, thus gaining more angular momentum than in the lower latitude. On the other hand, the reduction in rotation rate actually decreases the angular momentum of the whole planet, thus reduces the angular momentum obtained by the poleward moving jet stream. For the runs from 1Ω to $1/8\Omega$, the first factor dominates and the jet intensity gets stronger for smaller rotation rate. But for the $1/16\Omega$ run, the latter factor dominates and the angular momentum of the planetary rotation reduces a significant enough amount to offset the angular momentum increase caused by the poleward motion of the jet stream.

This poleward movement of the subtropical jet stream is a clear indication of the expansion of Hadley cell in each hemisphere as the rotation rate decreases, which can be found in Figure 5.4. The shaded variable plotted in this figure is the zonal mean meridional mass streamfunction, which is defined in the pressure coordinate system as (see *Peixoto and Oort* [1992];*Read* [2010]):

$$\Psi = \frac{2\pi a}{g}\cos\phi \int_0^P dp'[v]$$

or

$$\rho\mathbf{u} = \mathbf{j} \times \Psi$$

Where a is the planetary radius, $[v]$ is the zonal and temporal mean meridional velocity, ϕ is the latitude and ρ is the density of the air.

As we can see, there are basically three cells in each hemisphere for the terrestrial rotation rate ($\Omega^* = 1\Omega$). The positive values of Ψ represent counter-clockwise flow and the negative values represent clockwise flow, while the magnitude reflects the strength of the overturning. Thus the poleward edge of the overturning Hadley circulation can be estimated as the latitude of the boundary between the tropical cell and the adjacent mid-latitude cell. In this case (1Ω), the expansion of the Hadley cell in each hemisphere is roughly 30° which is consistent with the observational value for the Earth. As the rotation rate decreases, the overturning Hadley cell expands and gets intensified, just as predicted in the previously stated Held and Hou model (*Held and Hou* [1980]). In fact, at the lowest rotation rate $\Omega^* = 1/16\Omega$, only one strong hemispherically dominating Hadley cell is found in each hemisphere while the other two cells at mid- and high-latitude

disappear. Within the Hadley cell, baroclinicity (i.e. horizontal temperature difference in the meridional direction) is considerably small compared with that in the baroclinic eddy zones. This feature can be seen in the zonal mean temperature cross-sections in Figure 5.5.

There is a clear trend in the zonal mean temperature field from 8Ω to $1/16\Omega$ that the horizontal temperature gradient becomes smaller as the rotation rate decreases. This is especially prominent at the middle and high levels of the atmosphere, where the isothermal lines become almost horizontal parallels at the lower rotation rates, due to the strong and extending overturning Hadley circulation in each hemisphere which is highly efficient in smoothing out the horizontal temperature inhomogeneity. At higher rotation rates, the horizontal temperature variation shows staircase-like features, indicating the existence of zonally parallel baroclinic zones and belts, somewhat resembling the features of the Jovian atmosphere on the rapidly rotating gas giants.

5.3 Non-axisymmetric features—eddies and waves

It was not until the beginning of the 20th century that scientists finally realised that the global circulation can not be boldly simplified as an axisymmetric multi-cell circulation, and the large-scale (synoptic) eddies—cyclones and anticyclones are not just negligible perturbations to an idealised 'smooth' general circulation. For rapidly rotating planets like the Earth and Mars, the maintenance of the general circulation and the transport of heat and momentum depend significantly on the interactions between transient eddies and the mean flow. In the absence of eddies, the atmosphere of the mid- and high-latitudes would reach a state of radiative equilibrium, which is featured by larger horizontal temperature difference than what we observed and is baroclinically unstable. The baroclinic eddy transport of heat considerably reduces the equtor-to-pole temperature difference from that predicted by radiative equilibrium. Thus zonal mean diagnostics alone might not be enough to reveal the nature of the circulation regimes.

Here we employ a measure of wave activity the zonal wave number spectrum of the geopotential height at the 300mb level. Figure 5.6 and Figure 5.7 show the latitude-wavenumber plot of the geopotential height at the 300mb for different rotation rates. The wavenumber is calculated using Fast Fourier Transformation(FFT) method. At the terrestrial rotation rate (1Ω), the wave activities are focussed in the extratropical regions (roughly 30° poleward), with the most significant component of wavenumber 3 or so,

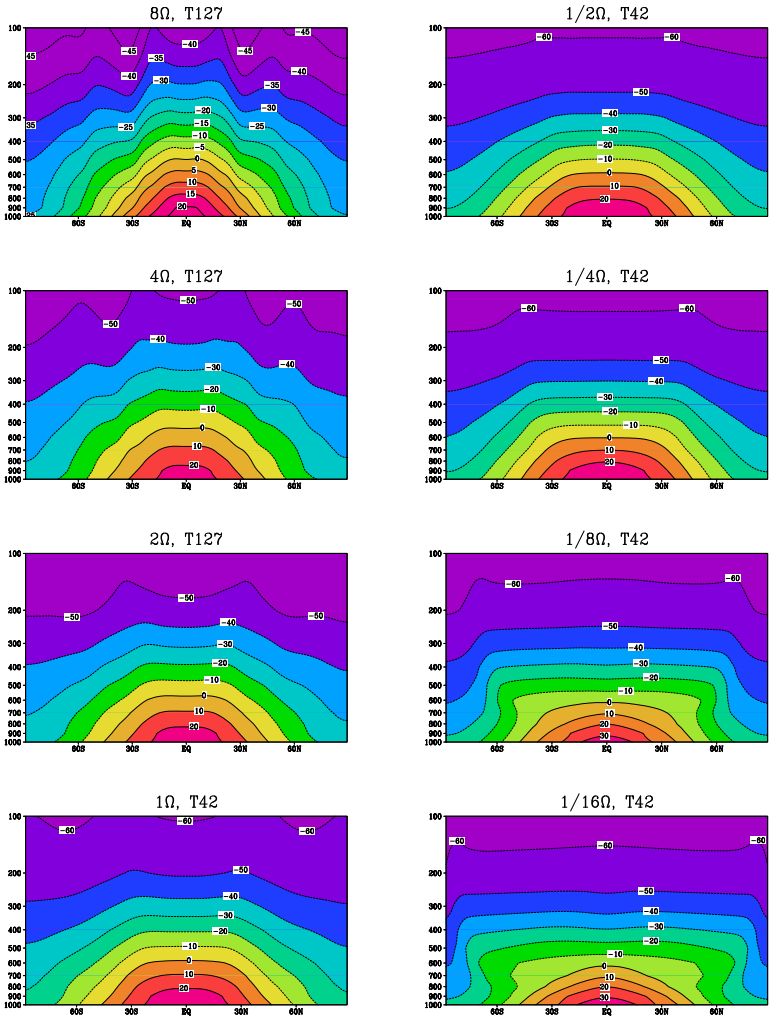

Figure 5.5: Zonal mean temperature field of 8Ω to 1/16Ω

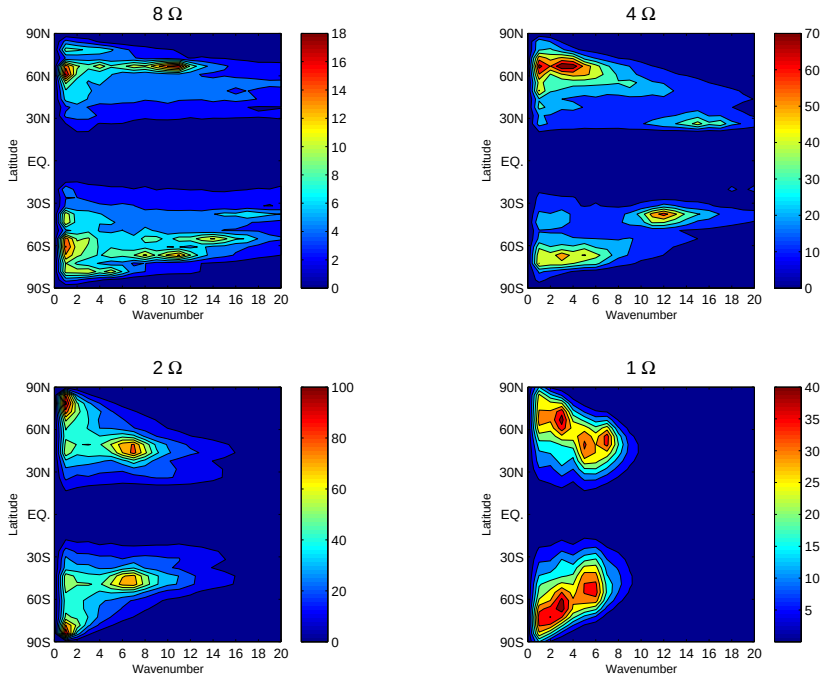

Figure 5.6: Latitude-wavenumber FFT spectrum of geopotential height at 300mb, 8Ω to 1Ω

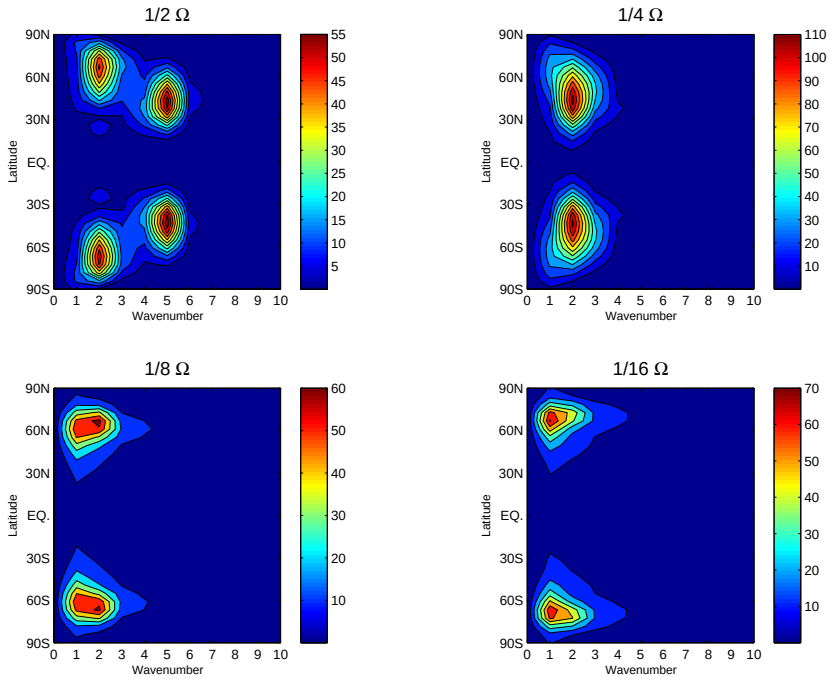

Figure 5.7: Latitude-wavenumber FFT spectrum of geopotential height at 300mb, 1/2Ω to 1/16Ω

while the total wavenumber spectrum spreads from wavenumber 0 to 10.

Increasing the rotation rate, we obtain a generally broader wavenumber spectrum in the extratropical area. Noticeable parallel zonal band features can be seen in the 8Ω spectrum, which indicates the existence of multiple baroclinic zones as a result of small Rossby deformation radius compared with the planetary radius. The magnitude of the FFT amplitude becomes small for higher rotation rate spectra. So the waves on a rapidly rotating planet(like that with 8Ω) are moving around the planet with small amplitude and are confined within separate zonal baroclinic zones, just like what we observed on the giant planets in our Solar System.

If we decrease the rotation rate, the spectrum shows a more complicated trend than those higher Ω spectra. At the rotation rate of $1/2\Omega$, we can see that the spectrum becomes more concentrated around the wavenumber 2 at high latitudes(about 60°) and the wavenumber 5 at mid-latidudes (about 45°), with the wavenumber 5 component stronger than that of the wavenumber 2. This reveals a highly regular and coherent flow regime. The amplitude of the waves reaches maximum at $1/4\Omega$ with the spectrum focusing around wavenumber 2. This is consistent with the trend that the Rossby deformation radius gets larger and larger as the rotation rate decreases. But if we go further to the spectrum of $1/8\Omega$ and $1/16\Omega$, the FFT amplitude actually decreases. This implies that the Rossby deformation radius under these slow rotation rates probably exceeds the planetary radius and baroclinic eddy development are suppressed within the planetary domain. And the wave activities appeared in $1/8\Omega$ and $1/16\Omega$ spectrums are probably due to barotropic instability, rather than baroclinic instability.

In order to qualitatively distinct the transition from baroclinic instability to barotropic instability (which occurs roughly between $1/4\Omega$ to $1/8\Omega$) as the rotation rate decreases, we introduce the zonally averaged transient eddy momentum and heat flux cross-sections as an index, as used by Geisler in his 1983 paper. Figure 5.8 shows the transient eddy heat and momentum flux for the terrestrial rotation rate (1Ω), representing the spatial pattern of the typical baroclinic eddy flux distribution. There is a maximum of eddy heat transport in the lower level at the poleward side of the mid-latidude jet, and an upper-level maximum of eddy momentum flux near the jet core. Following the reasoning of *Geisler et al.* [1983], we say that if the patterns of eddy heat and momentum fluxes resemble those shown in Figure 5.8, the waves are maintained by baroclinic processess; if the patterns differ significantly from those shown in Figure 5.8, then the waves and eddies should be due to barotropic instability.

The transient eddy momentum flux can be seen in Figure 5.9, which

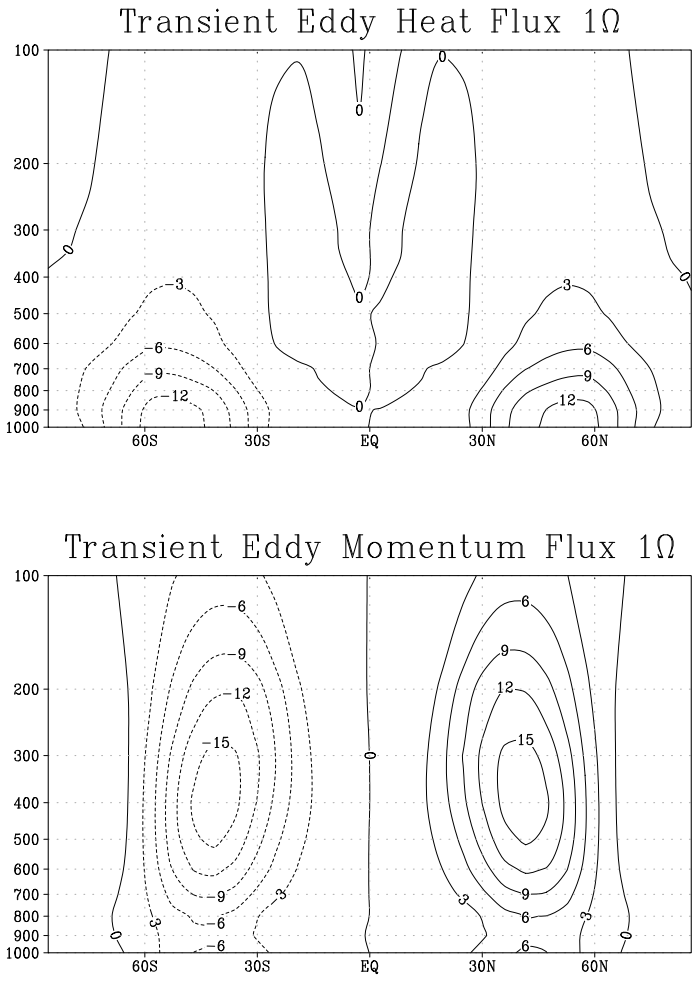

Figure 5.8: Zonal mean transient eddy flux of heat and momentum at the terrestrial rotation rate.

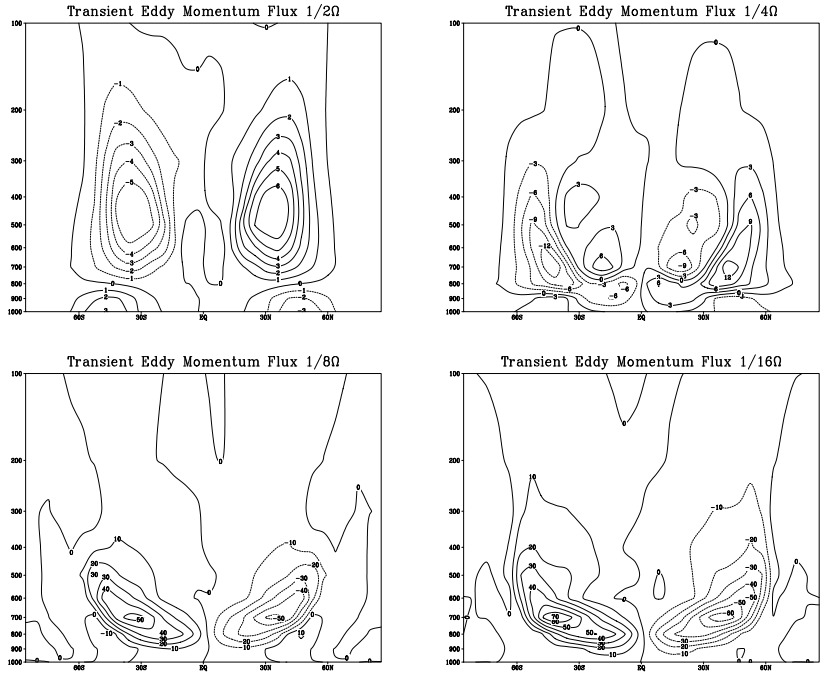

Figure 5.9: Eddy momentum flux cross-sections from 1/2Ω to 1/16Ω

shows a clear transition from 1/2Ω to 1/8Ω as the poleward eddy momentum transport converts to equatorward eddy momentum transport, with the pattern of 1/4Ω as a transitional form. We can thus say that the dynamical mechanism for the growth and maintenance of waves at 1/8Ω and 1/16Ω runs are dominated by barotropic instability.

One of the major features of baroclinic eddies is the tilted vertical structure of the eddy perturbation field. In Earth's atmosphere, mid-latitude cyclones and anticyclones has a westward tilt of pressure perturbation and an eastward tilt of temperature perturbation as one goes upwards from the ground level. A schematic of this kind of vertical structure can be seen in Figure 5.10.

This kind of vertical tilt is necessary for the release of available potential energy which is crucial for the growth of eddies induced by baroclinic instability. It's a common feature of stratified rotating fluid under the forcing of differential horizontal heating and can be found in laboratory experiments (as shown in Figure 5.11).

Vertical structures of geopotential height, temperature, vertical veloc-

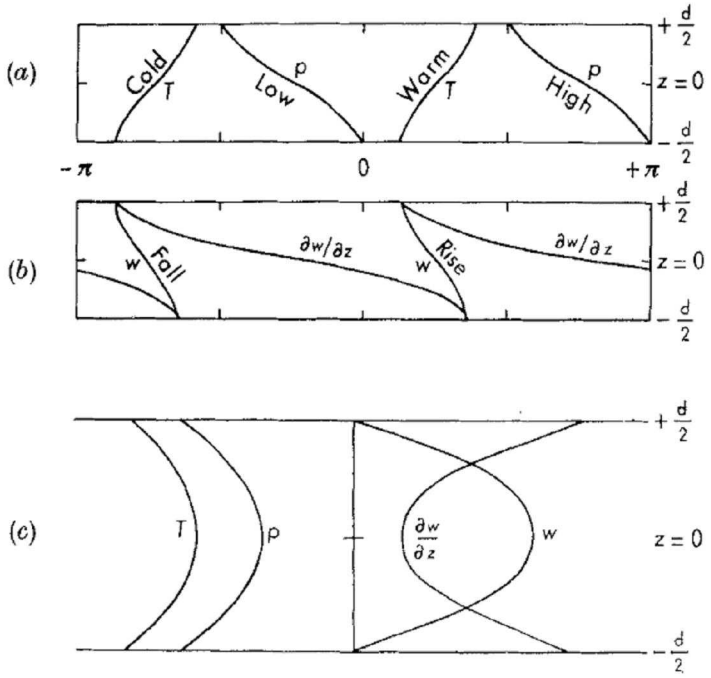

Figure 5.10: Schematic plot of the vertical structure of baroclinic waves, after *Eady* [1949]. (a) shows equal phase lines for the temperature and pressure fields; (b) shows equal phase lines of vertical velocity w and its vertical derivative $\partial w/\partial z$; and (c) shows the amplitude variations of $T, p, w, \partial w/\partial z$ in the vertical direction.

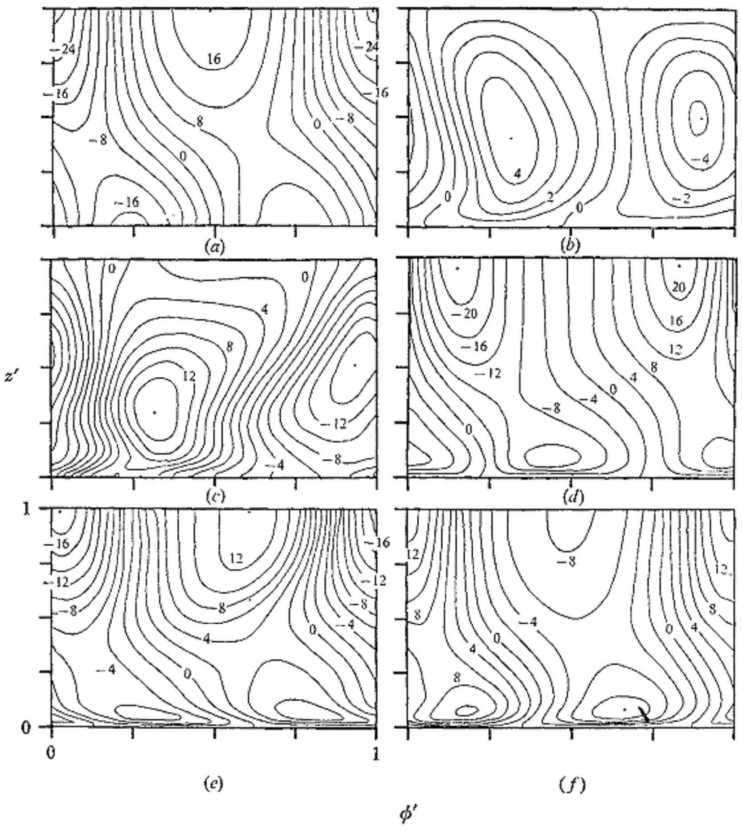

Figure 5.11: Laboratory examples of the vertical structure of baroclinic waves, after *Williams* [1971], *Hide and Mason* [1975]. The ordinate is z and the abscissa ϕ divided by one angular wavelength. Contours are in the azimuthal direction for (a) pressure perturbation, (b) vertical velocity, (c) fractional temperature perturbation, (d) radial velocity at $r = 1/2(a+b)$ and (e) and (f) the perturbation of the aximuthal velocity at $r = a + 1/4(b-a)$ and $r = a + 3/4(b-a)$.

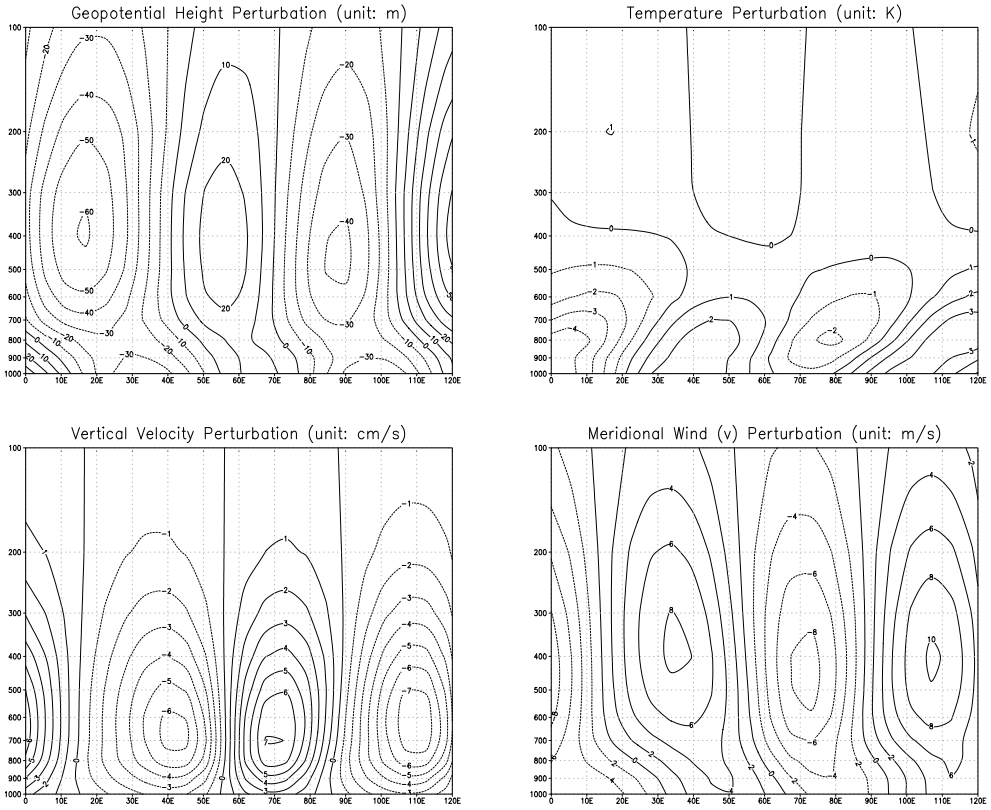

Figure 5.12: Vertical structure of the perturbation of the geopotential height, temperature, vertical and meridional velocity along the latitude 53N for $1/2\Omega$

ity, and meridional wind perturbations for the $1/2\Omega$ to $1/16\Omega$ runs can be found in Figures 5.11-14. From the surface to middle level of the troposphere (apporximately 500mb), we can clearly see a westward tilt in the pressure perturbation field and an eastward tilt in the temperature perturbation field for the $1/2\Omega$ run, which are consistent with those shown in Figure 5.11, indicating that baroclinic processes are dominating here. For the $1/8\Omega$ and $1/16\Omega$ runs, such vertical tilt can be barely seen, implying barotropic structure.

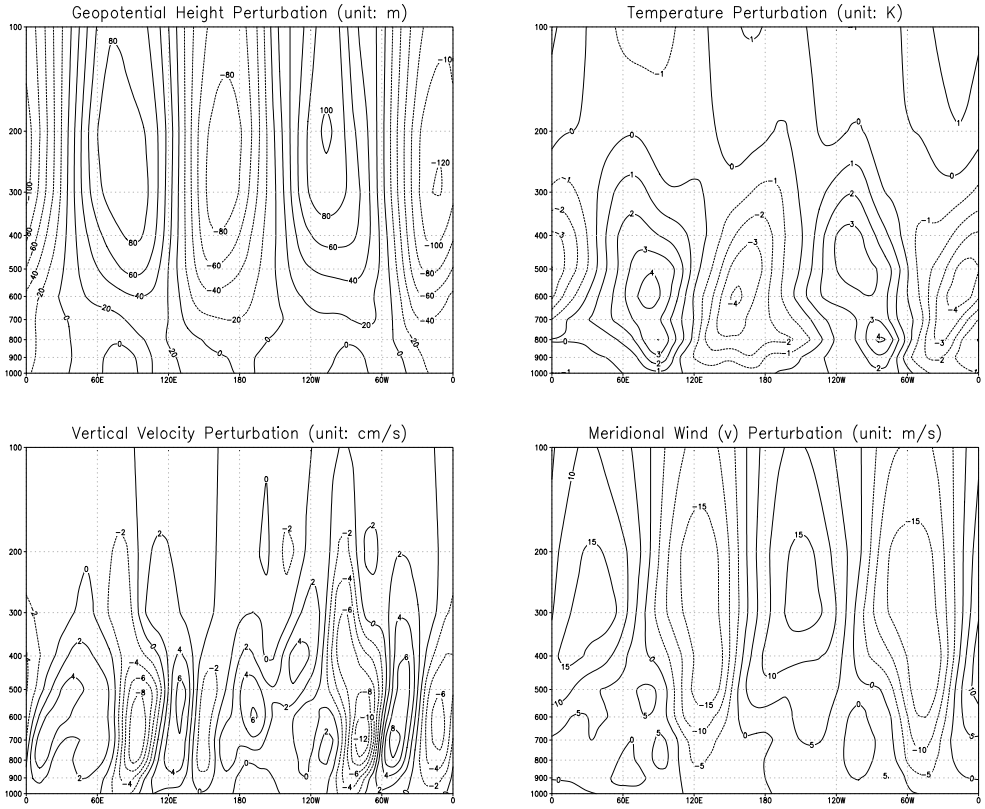

Figure 5.13: Same as Figure 5.12, but for 1/4Ω

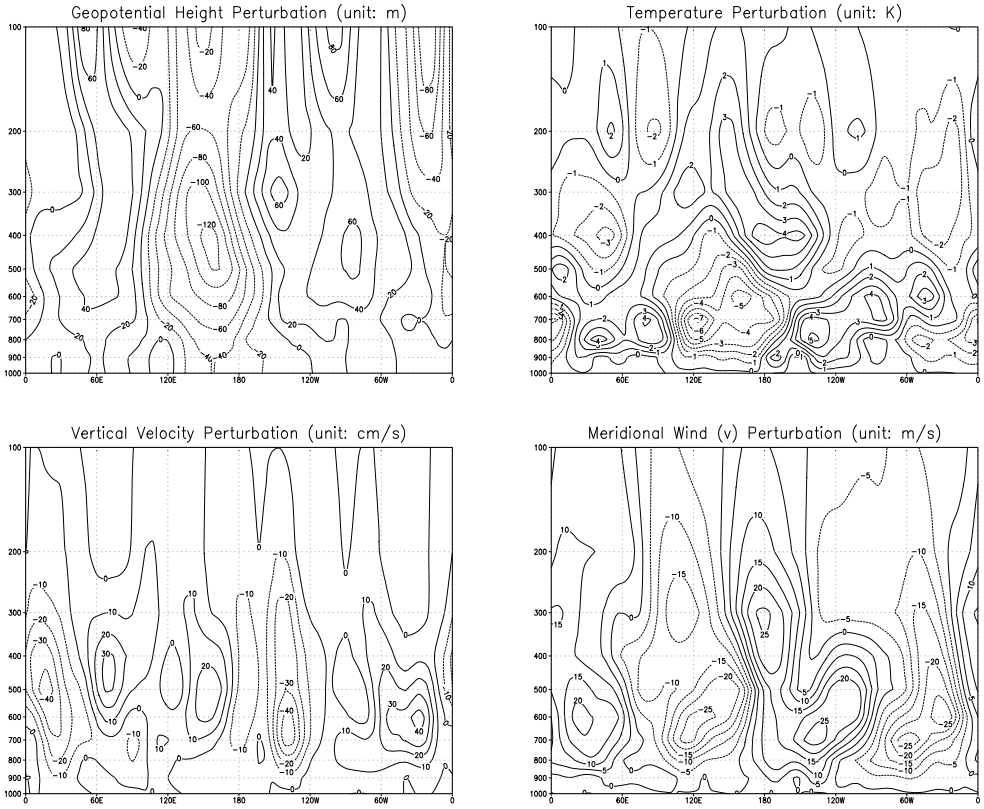

Figure 5.14: Same as Figure 5.12, but for 1/8Ω

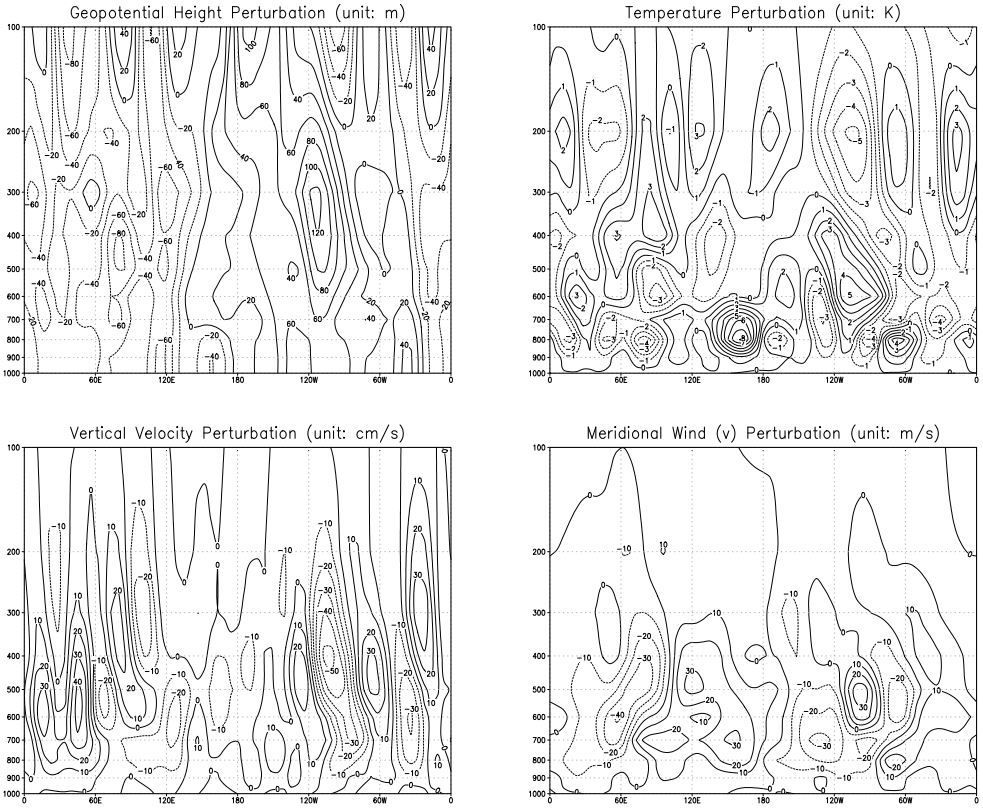

Figure 5.15: Same as Figure 5.12, but for 1/16Ω

5.4 Runs with a smaller planetary radius

Changing the planetary radius is actually another way to change the value of the thermal Rossby number, whilst keeping the corresponding radiative relaxational timescale and the Rayleigh frictional timescale, which always need to be changed if we change the rotation rate while trying to keep the absolute values of these timescales the same. According to the expression of thermal Rossby number,

$$\mathcal{R}o \simeq \frac{U_T}{\Omega L} = \frac{g\alpha\Delta T\Delta D}{\Omega^2 L^2},$$

we know that the decrease of planetary radius is equivalent to the decrease of planetary rotation rate. It would thus be reasonable to anticipate that circulation patterns of $1/16\Omega$ and $1/16a$ should not differ very much from each other. This idea is inspired by the investigation of Mitchell and Vallis (see *Mitchell and Vallis* [2010]) on the relationship between superrotation and thermal Rossby number. But what we obtained shows that the circulation patterns of these two scenarios are significantly different from each other.

Figure 5.16 shows the zonal mean temperature cross-section of the mini Earth ($a = 400km$, that is, 1/16 of that of the normal Earth) experiment. We can see that the horizontal temperature difference between the equator and the pole is much smaller than that observed in the previously stated $1/16\Omega$ experiment (shown in Figure 5.4 and Figure 5.5). And this small meridional temperature gradient actually fits much better with our theoretical predictions for slowly rotating planets, compared with the trend we found when decreasing the rotation rate.

The zonal mean zonal wind field of this mini Earth is featured by a strong and well-defined equatorial superrotation flow which makes the global circulation pattern looks more like what we observed on Venus and Titan, again showing great advantage over the $1/16\Omega$ experiment. These differences between mini Earth runs and decreased rotation rate runs indicate that there are perhaps other dimensionless parameters yet to be discovered which might exert great constraints on the global circulation regimes of terrestrial planets. However, it should not be neglected that there is another possiblity for this inconsistence, which is associated with the scaling of the vaiables in PUMA during the model calculation. In PUMA, all the equations and variables are non-dimensionalised before integration is conducted. For example, temperature is scaled by $a^2\Omega^2/R$, geopotential Φ by $a^2\Omega^2/g$, where a is the planetary radius, R the gas constant of dry air, and g the

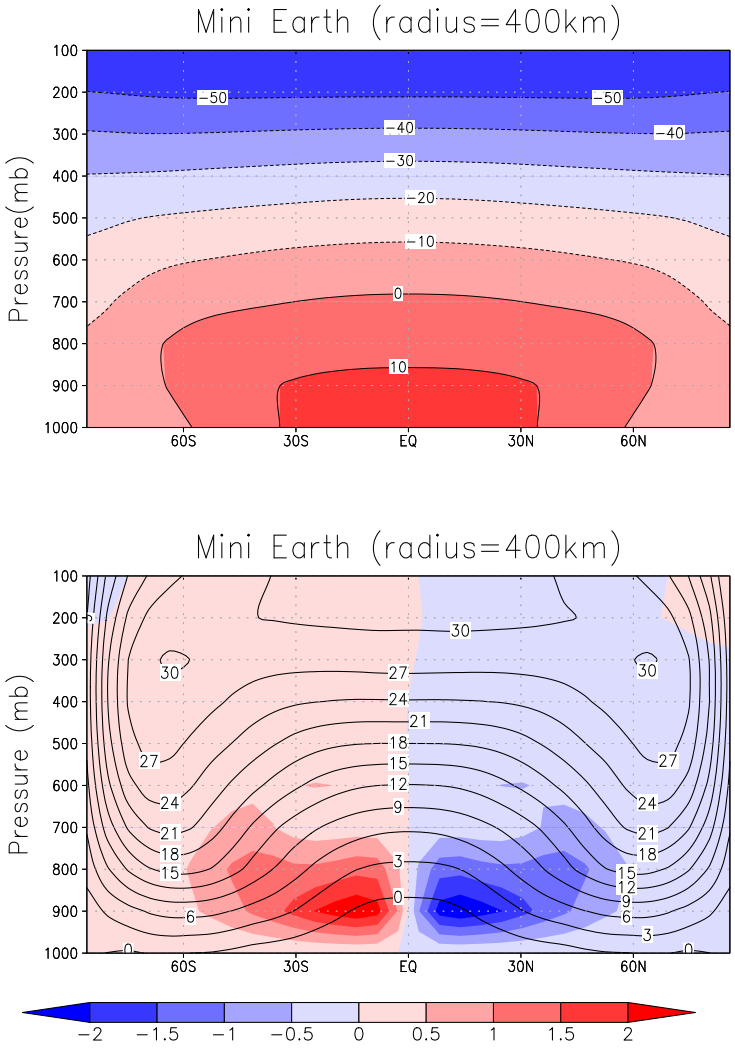

Figure 5.16: Zonal mean temperature, zonal wind, and the meridional mass streamfunction for the mini Earth run (planetary radius=400km)

Ω/Ω_E	$\mathcal{R}_o$	N_J	F_f
1/16	20.25	0.14	0.62
1/8	5.06	0.28	2.48
1/4	1.27	0.57	9.92
1/2	0.32	1.13	39.67
1	0.079	2.26	158.69
2	0.020	4.53	634.75
4	0.005	9.06	2.54×10^3
8	0.001	18.08	1.02×10^5

Table 5.1: Dimensionless numbers of the $1/16\Omega$ to 8Ω experiments

gravitational acceleration. When we change the values of planetary radius or the planetary rotation rate, we might have caused other variables changed through the scaling. Therefore, it will be worthwhile in the next stage to look back into the model source code to find out whether it is safe to directly change the value of either planetary radius or rotation rate without causing undesirable changes.

5.5 Discussion on dimensionless numbers

In this section we present the estimates of the characteristic non-dimensional numbers of our experiments of changing the planetary rotation rate, as shown in Table 5.1.

Here the number of jets is estimated by

$$N_J = \frac{a}{L_R} = \frac{2}{\pi\sqrt{\mathcal{R}_o}}$$

where a is the radius of the planet, L_R the Rhines scale, and $\mathcal{R}_o$ the thermal Rossby number. a can be viewed as the characteristic length scale of the planetary domain, while L_R can be viewed as the characteristic meridional scale of the β plane baroclinic eddies.

As we can see, in the terrestrial case($\Omega/\Omega_E = 1$), the number of jet streams is between 2 and 3, indicating that the Earth is actually a bit beyond the regime where only one jet stream can exist in each hemisphere. These estimates are in reasonable agreement with those produced by *Read* [2010] based on the experiments of *Williams* [1988a], as shown in the following Table 5.2. The onset of baroclinic instability occurs when $\mathcal{R}_o < 1$,

Ω/Ω_E	$\mathcal{B}_u$	$\mathcal{R}_o$	N_J	F_f
1/16	10.1	12.0	0.18	4
1/8	2.8	3.3	0.35	15
1/4	0.63	1.0	0.63	62
1/2	0.16	0.21	1.4	247
3/4	0.08	0.083	2.2	555
1	0.048	0.053	2.7	987
2	0.012	0.016	5.0	3950
4	0.003	0.006	8.3	1.6×10^4
8	0.0008	0.002	13.7	6.3×10^4

Table 5.2: Dimensionless numbers calculated by *Read* [2010], based on experiments of *Williams* [1988a]

which corresponds to $\Omega > 1/4\Omega_E$. This fits well with the previously stated transition of instability around $1/4\Omega_E$.

Chapter 6

Conclusions and Future Work

6.1 Conclusions

This report presents the work done within my first year on the parametric dependence of the terrestrial planetary circulation regimes on the dimensionless planetary parameters. A simplified general circulation model PUMA is employed to conduct a series of controlled experiments on planetary parameters like rotation rate and the prescribed equator-to-pole temperature difference. This parametric approach, either laboratorially or numerically, has a long history in the study of geophysical fluid dynamics. What we are trying to do in this project, is to establish a comprehensive parameter space (probably more than three dimensions) in which the occurences of a wide range of planetary circulation patterns are mapped with repect to the corresponding parameters. This sort of regime diagram, once established, will provide an invaluable pool of references for the future research of the circulation and even climate conditions on terrestrial exoplanets. In order to make sure that such numerical experiments are generic enough to be relevant to other terrestrial planets, we choose the highly simplified GCM—PUMA as our major platform. With a generally linear physics scheme (Newtonian cooling and Rayleigh friction), PUMA can be essentially viewed as a PDE solver for dry ideal atmosphere within a rotating spherical shell.

The investigation of the dependence of the global circulation regime on planetary rotation rate is the major part of the work done in the first year. Rotation is the cause of various unique features for planetary atmospheres that differs significantly from non-rotating fluids. Thus it is natural to choose

rotation rate as the starting point for our systematic exploration across the multi-dimensional parameter space. The trend we observed is that Hadley cell expands and subtropical jet stream goes poleward as the planetary rotation slows down; multiple jets, like what we observed on giant planets in our Solar System, can be found when the rotation rate exceeds twice of the Earth's rotation rate; the dominating instability mechanism for the formation and maintenance of eddies transits from baroclinic to barotropic (or probably a mixing of baroclinic and barotropic) as the rotation rate decreases. These qualitative trends fit well with the theoretical predictions made for either axisymmetric circulation (see *Held and Hou* [1980]) or non-axisymmetric wavy circulation(see *Rhines* [1975]).

The regime diagram we finally obtained is a two-dimensional parameter plane constructed by thermal Rossby number and the sqaure of the rotation rate(which acts as a substitute of $\mathcal{F}_r$ and $\mathcal{F}_f$). A slant boundary between the axisymmetric and non-axisymmetric flow regimes can be found in the lower part of the regime diagram, which is more or less consistent with the previous work done by *Geisler et al.* [1983]. Compared with the regime diagram obtained by *Hide and Mason* [1975] for rotating annulus, this regime diagram has no upper symmetric region (the axisymmetric flow region above the turning point of the boundary curve). This absence of upper symmetric region is probably due to the geometric difference between spherical shell and the cylindrical annulus. Within the cylindrical annulus, the jet stream can not move close to the axis and get intensified due to the confinement of the inner cylinder, thus suppressing the growth of barotropic instability (which would otherwise be resulted from the horizontal speed shear around the strong jet) at the low rotation rate, leading to axisymmetric flows at the upper symmetric region.

The question of what characteristic parameters define the general circulation possibly has not yet been fully answered so far. A lot of other planetary factors like the obliquity of the spin axis, the radiative properties of the atmosphere and so forth also play a significant role in shaping the global circulation and need to be taken into account. These outstanding topics will be investigated in the subsequent years.

6.2 Future Work

The next step in exploring the parameter space is to investigate the influence of the radiative properties of the atmosphere on global circulation regime. The current parametrisation of diabatic forcing is Newtonian cooling with a

prescribed equilibrium temperature field defined for the Earth, which should be replaced by a more physically realistic representation that is not peculiar to a specific planet. News from the Hamburg group suggests that such kind of simplified radiation codes to complement PUMA are under development right now, and we anticipate to employ their codes in our future study for convenience, although the potential need to develop our own codes still exists since we have no idea how soon the German codes will be released. We are planning to add a two-band radiative-convective scheme consisting of the transfer of longwave(infrared) and shortwave(stellar) radiation. By specifying the values of the total atmospheric optical depth in these two bands as well as the surface albedo, we can deduce a more reasonable vertical temperature structure (presumably an isothermal stratosphere with a troposphere of constant lapse rate beneath it) than simply relaxing the temperature field towards a prescribed radiative equilibrium field.

The characteristic non-dimensional parameters that we expect to construct must fully reflect the radiative properties of this two-band atmosphere (the atmosphere can be viewed as a grey absorber in each band, that is, constant transmission for longwave and shortwave respectively). The total optical depth of the atmosphere as well as the ratio of the optical depth for longwave and shortwave radiation can be used as two independent dimensionless parameters. If the ratio is greater than unity (that is, the atmosphere is optically thick in the longwave band and thin in the shortwave band), then greenhouse effect is expected to exist. If the ratio is less than unity(that is, the atmosphere is optically thin in the longwave band and thick in the shortwave band), then the atmosphere would turn out to be heated from the above and would thus be presumably more stable. Studies of the parametric dependence of the Hadley cell has been conducted by *Caballero et al.* [2008] using this kind of simplified non-grey radiation code, and would thus provide a beneficial reference for our future work of upgrading our simplified GCM to encompass the radiation effects.

It should be pointed out that it is highly desirable for us to keep the number of characterising dimensionless parameters as few as possible, since the computational cost of the new controlled experiments brought by adding new dimensions to a parameter space will be fairly formidable, especially when the parameter space has already grown to have multiple dimensions. Thus the construction of dimensionless parameters should be taken with great caution and consideration.

Works in the far future will also include the orbital parameters like planetary obliquity, orbital eccentricity and so on to encompass the fairly extraodinary planetary conditions that might be encountered on exoplanets (for

example, tidally-locked state, see *Cho* [2008], *Joshi et al.* [1997]; or extreme obliquity, see *Williams and Pollard* [2003]). What we are hoping to achieve at the end of this project is to provide a broad spectrum of the potential terrestrial circulation patterns, which we hope would serve as a quantitative (or at least semi-quantitative) reference for scientists in the exoplanet community on issues related to the climate or even potential habitability to terrestrial organisms on those exotic worlds.

6.3 Preliminary Timetable

The preliminary timetable for the forthcoming years is listed in the following:

Oct.2010—Dec.2010	Development of the two-band radiation code for PUMA
Jan.2011—Mid.2011	Controlled experiments on radiative parameters and the frictional parameters
Mid.2011—End.2011	Experiments on obliquity and orbital parameters with considerations on special scenarios like tidally locked states
End.2011—Mid 2012	Finalise the results and write the thesis

Bibliography

Barry, L., G. C. Craig, and J. Thuburn, Poleward heat transport by the atmospheric heat engine, *Nature*, *415*, 774–777, 2002.

Bastin, M. E., and P. L. Read, Experiments on the structure of baroclinic waves and zonal jets in an internally heated, rotating, cylinder of fluid, *Physics of Fluids*, *10*, 374–389, 1998.

Caballero, R., R. T. Pierrehumbert, and J. L. Mitchell, Axisymmetric, nearly inviscid circulations in non-condensing radiative-convective atmospheres, *Quarterly Journal of the Royal Meteorological Society*, *134*, 1269–1285, 2008.

Cho, J., Atmospheric dynamics of tidally synchronized extrasolar planets, *Royal Society of London Philosophical Transactions Series A*, *366*, 4477–4488, 2008.

Del Genio, A. D., and R. J. Suozzo, A comparative study of rapidly and slowly rotating dynamical regimes in a terrestrial general circulation model, *Journal of Atmospheric Sciences*, *44*, 973–986, 1987.

Dowling, T. E., Dynamics of jovian atmospheres, *Annual Review of Fluid Mechanics*, *27*, 293–334, 1995.

Eady, E. T., Long waves and cyclone waves, *Tellus*, *1*, 33–52, 1949.

Frierson, D. M. W., J. Lu, and G. Chen, Width of the Hadley cell in simple and comprehensive general circulation models, *Geophysical Research Letters*, *34*, 18,804–+, 2007.

Fultz, D., R. Long, G. Owens, W. Bowen, R. Kaylor, and J. Weil, Studies of thermal convection in a rotating cylinder with some implications for large-scale atmospheric motions, *Meteorological Monographs American Meteorological Society*, *4*, 1959.

Geisler, J. E., E. J. Pitcher, and R. C. Malone, Rotating-Fluid experiments with an atmospheric general circulation model, *Journal of Geophysical Research*, *88*, 9706–9716, 1983.

Green, J. S. A., Transfer properties of the large-scale eddies and the general circulation of the atmosphere, *Quarterly Journal of the Royal Meteorological Society*, *96*, 157–185, 1970.

Hadley, G., Concerning the Cause of the General Trade-Winds: By Geo. Hadley, Esq; F. R. S., *Royal Society of London Philosophical Transactions Series I*, *39*, 58–62, 1735.

Hayashi, Y. Y., K. Ishioka, M. Yamada, and S. Yoden, Emergence of circumpolar vortex in two dimensional turbulence on a rotating sphere, *Proceedings of the IUTAM Symposium on Developments in Geophysical Turbulence (Fluid Mechanics and its Application)*, *58*, 179–192, 2000.

Held, I. M., The macroturbulence of the troposphere, *Tellus Series A*, *51*, 59–+, 1999.

Held, I. M., *The general circulation of the atmosphere*, Paper presented at 2000 WHOI GFD program, Woods Hole Oceanography Institute, Woods Hole, MA, 2000.

Held, I. M., and A. Y. Hou, Nonlinear Axially Symmetric Circulations in a Nearly Inviscid Atmosphere., *Journal of Atmospheric Sciences*, *37*, 515–533, 1980.

Held, I. M., and V. D. Larichev, A Scaling Theory for Horizontally Homogeneous, Baroclinically Unstable Flow on a Beta Plane, *Journal of Atmospheric Sciences*, *53*, 946, 1996.

Hide, R., Some experiments on thermal convection in a rotating liquid, *Quarterly Journal of the Royal Meteorological Society*, *79*, 161–161, 1953.

Hide, R., *Some laboratory experiments on free thermal convection in a rotating fluid subject to a horizontal temperature gradient and their relation to the theory of the global atmospheric circulation.In: Corby, G.A.(Ed.), The Global Circulation of the Atmosphere.*, Royal Meteorological Society, London, 1969.

Hide, R., and P. J. Mason, Sloping convection in a rotating fluid, *Advances in Physics*, *24*, 47–100, 1975.

Holton, J., *An Introduction to Dynamic Meteorology, fouth ed.*, Elsevier Academic Press, 2004.

Hoskins, B. J., and A. J. Simmons, A multi-layer spectral model and the semi-implicit method, *Quarterly Journal of the Royal Meteorological Society*, *101*, 637–655, 1975.

Hunt, B. G., The Influence of the Earth's Rotation Rate on the General Circulation of the Atmosphere., *Journal of Atmospheric Sciences*, *36*, 1392–1408, 1979.

Illari, L., et al., "WEATHER IN A TANK"Exploiting Laboratory Experiments in the Teaching of Meteorology, Oceanography, and Climate, *Bulletin of the American Meteorological Society*, *90*, 1619–+, 2009.

Irwin, J., D. Charbonneau, P. Nutzman, and E. Falco, The MEarth project: searching for transiting habitable super-Earths around nearby M dwarfs, in *IAU Symposium*, vol. 253 of *IAU Symposium*, pp. 37–43, 2009.

James, I., *Introduction to Circulating Atmospheres*, Cambridge University Press, UK, 1994.

Jenkins, G., A sensitivity study of changes in Earth's rotation rate with an atmospheric general circulation model, *Global and Planetary Change*, *11*, 141–154, 1996.

Joshi, M. M., R. M. Haberle, and R. T. Reynolds, Simulations of the Atmospheres of Synchronously Rotating Terrestrial Planets Orbiting M Dwarfs: Conditions for Atmospheric Collapse and the Implications for Habitability, *Icarus*, *129*, 450–465, 1997.

Lee, C., S. R. Lewis, and P. L. Read, A numerical model of the atmosphere of Venus, *Advances in Space Research*, *36*, 2142–2145, 2005.

Lewis, S. R., M. Collins, P. L. Read, F. Forget, F. Hourdin, R. Fournier, C. Hourdin, O. Talagrand, and J. Huot, A climate database for Mars, *Journal of Geophysical Research*, *104*, 24,177–24,194, 1999.

Lorenz, E., *The Nature and Theory of the General Circulation of the Atmosphere*, No.218.W.M.O.,Geneva, 1969.

Mitchell, J., and G. Vallis, The transition to superrotation in terrestrial atmospheres, *Journal of Geophysical Research*, 2010.

Navarra, A., and G. Boccaletti, Numerical general circulation experiments of sensitivity to Earth rotation rate, *Climate Dynamics*, *19*, 467–483, 2002.

Peixoto, J., and A. Oort, *Physics of climate*, Springer, 1992.

Read, P., Dynamics and circulation regimes of terrestrial planets, *Planetary and Space Science*, 2010.

Read, P., and S. Lewis, *The Martian Climate Revisited: Atmosphere and Environment of a Desert Planet*, Springer-Praxis, 2004.

Read, P. L., Super-rotation and diffusion of axial angular momentum. II. A review of quasi-axisymmetric models of planetary atmospheres., *Quarterly Journal of the Royal Meteorological Society*, *112*, 253–272, 1986.

Read, P. L., Transition To Geostrophic Turbulence In The Laboratory, And As A Paradigm In Atmospheres And Oceans, *Surveys in Geophysics*, *22*, 265–317, 2001.

Read, P. L., M. Collins, W. Fruh, S. R. Lewis, and A. F. Lovegrove, Wave interactions and baroclinic chaos: a paradigm for long timescale variability in planetary atmospheres., *Chaos Solitons and Fractals*, *9*, 231–249, 1998.

Rhines, P. B., Waves and turbulence on a beta-plane, *Journal of Fluid Mechanics*, *69*, 417–443, 1975.

Selsis, F., J. F. Kasting, B. Levrard, J. Paillet, I. Ribas, and X. Delfosse, Habitable planets around the star Gliese 581?, *Astronomy and Astrophysics*, *476*, 1373–1387, 2007.

Showman, A., J.-K. Cho, and K. Menou, *Atmospheric circulation of exoplanets, In: Seager, S. (Ed.), Exoplanets.*, University of Arizona Press, Tucson, Arizona, 2010.

Stone, P. H., A simplified radiative-dynamical model for the static stability of rotating atmospheres., *Journal of Atmospheric Sciences*, *29*, 405–418, 1972.

Stone, P. H., Baroclinic Adjustment., *Journal of Atmospheric Sciences*, *35*, 561–571, 1978.

Sukoriansky, S., N. Dikovskaya, and B. Galperin, On the Arrest of Inverse Energy Cascade and the Rhines Scale, *Journal of Atmospheric Sciences*, *64*, 3312–+, 2007.

Williams, D. M., and D. Pollard, Extraordinary climates of Earth-like planets: three-dimensional climate simulations at extreme obliquity, *International Journal of Astrobiology*, *2*, 1–19, 2003.

Williams, G. P., Baroclinic annulus waves, *Journal of Fluid Mechanics*, *49*, 417–449, 1971.

Williams, G. P., The dynamical range of global circulationsI, *Climate Dynamics*, *2*, 205–260, 1988a.

Williams, G. P., The dynamical range of global circulations II, *Climate Dynamics*, *3*, 45–84, 1988b.

Williams, G. P., and J. L. Holloway, The range and unity of planetary circulations, *Nature*, *297*, 295–299, 1982.

Wordsworth, R. D., P. L. Read, and Y. H. Yamazaki, Turbulence, waves, and jets in a differentially heated rotating annulus experiment, *Physics of Fluids*, *20*, 126,602–+, 2008.

Yoden, S., K. Ishioka, Y. Y. Hayashi, and M. Yamada, A further experiment on two-dimensional decaying turbulence on a rotating sphere, *Nuovo Cimento C Geophysics Space Physics C*, *22*, 803–812, 1999.